



401 N. Lindbergh Blvd.  
St. Louis, MO 63141  
Tel.: 314.993.1700, #546  
Toll Free: 800.424.2841, #546  
Fax: 800.708.1364

Send via email to: [jbode@aaortho.org](mailto:jbode@aaortho.org) and [cyoung@aaortho.org](mailto:cyoung@aaortho.org)

**AAO Foundation Final Report Form**  
**(a/o 5/30/2021)**

Type of Award, Orthodontic Faculty Development Fellowship Award,

Name(s) of Principal Investigator(s) Siddharth Vora

Institution University of British Columbia

Title of Project Role of Colony Stimulating Factor -1 Receptor in Odontogenesis

Period of AAOF Support July-2019 to June-2021

Amount of Funding \$20,000

Summary/Abstract

Odontogenesis occurs via a complex sequence of epithelial-mesenchymal interactions which ultimately result in the formation of specialized mineralized tissues by highly differentiated cells. A coordinated cascade of gene expression events regulate all aspects of tooth formation, including number, location, size, morphology as well as the physical and mechanical properties of mineralized tissues. While several key genetic players regulating odontogenesis have been identified and studied, the role of many more genes and molecules in this process remain undetermined. This study investigated the potential role of Colony Stimulating Factor 1 Receptor (CSF1R) during odontogenesis. We first evaluated the expression of CSF1 and CSF1R in developing dental tissues during fetal and perinatal stages, using immunofluorescence. We found a gradual increase in CSF1R expression from embryonic day 13.5 to postnatal day 5 in the ectomesenchyme derived dental follicular and pulpal tissues, with no expression within the odontogenic epithelium. PLX5622, a highly specific CSF1R inhibitor was fed to pregnant CD1 mice from e3.5-e18 and pups were examined at fetal and perinatal timepoints to study tooth and bone formation. CSF1R inhibited mice displayed shortened incisors with an apparent lack of adequate bone remodeling around the cervical loop regions. Similarly, developing molars were constricted in the buccolingual dimension with excess bone formation, particularly on the buccal surfaces at e18. TRAP staining revealed a concomitant reduction in osteoclastic activity in

CSF1R inhibited mice at embryonic and early postnatal stages. 3D morphological analysis at postnatal day 21 revealed tooth size and shape abnormalities in-line with those observed in utero. Briefly, maxillary incisors showed notching, ectopic enamel ridges as well as twinning on the superior surface. Mandibular incisors showed notching and extensive infoldings of the odontogenic epithelium. In both arches' incisors were smaller in length. Additionally, maxillary and mandibular first molars showed narrowing in the buccolingual dimension and elongation in the mesio-distal dimension, with taurodontic roots in mandibular first molars. Surprisingly, CSF1R inhibition in adult mice (P21) for 4 weeks did not show any disruptions in incisor tooth elongation using uCT analysis. Together, these data suggest that CSF1R plays an important role in the dental follicular regions surrounding the developing enamel organs during fetal stages, likely via osteoclast induced bone remodeling. Early disruption of CSF1R activity can impact normal dental morphogenesis, however, teeth continue to develop and erupt. Future studies will be aimed at dissecting precise mechanisms via which CSF1R regulates odontogenesis.

Detailed results and inferences:

1. If the work has been published please attach a pdf of manuscript OR
2. Describe in detail the results of your study. The intent is to share the knowledge you have generated with the AAOF and orthodontic community specifically and other who may benefit from your study. Table, Figures, Statistical Analysis, and interpretation of results should be included.

Relevant sections of MSc Thesis of Ashina Nagra has been submitted. These data, along with additional data, are currently being compiled for publication (see below).

Respond to the following questions:

1. Were the original, specific aims of the proposal realized?

*Educational:* I continued to gain skills in the use of R for statistical and morphometric analyses. For the latter, I attended a 5-day intensive workshop on geometric morphometrics using R (Transmitting Science). This course was the second one I have attended on this topic and has advanced my skill in the use of these methods. I also attended grantsmanship workshops, knowledge translation to improve my scholarly and mentorship abilities.

*Research:* We were able to complete Aim 1 of the study as well as parts of Aim 2a and aim 2c (see MSc Thesis). Due to culling of animals at the beginning of Covid19 lockdown periods, we were unable to complete parts of Aims 2a and Aim 2b. These studies will be undertaken next.

*Teaching:* I continued to engaged in undergraduate and graduate teaching activities at the UBC's FOD. I also uploaded extensively scripted and edited teaching material pertaining to Craniofacial Embryology and Odontogenesis to my hosted website– Ortholectures.com. This allowed for seamless access to videos for self-learning of material and greatly supplemented students educational experience. I also continued to mentor several students including 3 who graduated – Dr. Beatriz Fortanely- MSc in Orthodontics, Dr. Raid Khayat-MSc in Craniofacial Biology and Ashina Nagra- MSc in Cell and Developmental Biology. I also attended Workplace Engagement workshops to improve my mentorship skills

*Clinical:* I completed by ABO board certification in 2020. I was unable to continue clinical activity since Feb 2020 since the Canadian-USA border was closed due to Covid travel restrictions. Hence, I had to give up my clinical practice in Bellingham, WA. I have recently began private practice in Vancouver BC.

2. Were the results published? – Not yet (see below)
  - a. If so, cite reference/s for publication/s including titles, dates, author or co-authors, journal, issue and page numbers – N/A
  - b. Was AAOF support acknowledged? – AAOF support will be acknowledge in planned publication (see below)
  - c. If not, are there plans to publish? If not, why not?

The data from the study is being currently compiled for publication and will be submitted by mid-December 2021. Our target journal is *Frontiers in Genetics* – special edition on “Genetics of Craniofacial and Neurodevelopmental Disorders: Insights from Cell and Developmental Biology”.

3. Have the results of this proposal been presented? Yes
  - a. If so, list titles, author or co-authors of these presentation/s, year and locations
    - Nagra, A; Rosin, J; Vora, SR. The Role of CSF1R in Early Tooth Development. *Experimental Biology*. April 2021 Meeting - Anatomy (online)
    - Nagra, A; Rosin, J; Kurrasch, D; Richman, J; Vora, SR. Osteoclast Activity in Early Tooth Morphogenesis. *International Association of Dental Research (IADR) Annual Conference July 2021* (online)
    - Siarkowski, M\*; Chen, L; Rosin, J; Kurrasch, D; Vora, S. Embryonic CSF-1 receptor inhibition results in dental malformations in mice. *International Association of Dental Research*. 2019, Vancouver BC.
  - b. Was AAOF support acknowledged? Yes
  - c. If not, are there plans to do so? If not, why not? N/A

To what extent have you used, or how do you intend to use, AAOF funding to further your career?

Continued support from the AAOF has enabled me to sustain an academic career. Previous support from the AAOF has been critical in my pursuit of a post-doc and provided encouragement to pursue a junior faculty position. I believe that the AAOF’s support will continue to be crucial to my future goals of obtaining independent research funding. I thank the foundation, the PARC committee and all of its champions and hope to continue a positive relationship with this organization.

Accounting for Project; (i.e.), any leftover funds, etc. – None

**THE ROLE OF CSF1R IN EARLY TOOTH DEVELOPMENT**

by

Ashina Nagra

B.Sc., Simon Fraser University, 2018

A THESIS SUBMITTED IN PARTIAL FULFILLMENT OF  
THE REQUIREMENTS FOR THE DEGREE OF

MASTER OF SCIENCE

in

The Faculty of Graduate and Postdoctoral Studies  
(Cell and Developmental Biology)

THE UNIVERSITY OF BRITISH COLUMBIA  
(Vancouver)

August 2021

© Ashina Nagra, 2021

## **Chapter 2: Materials and Methods**

### **2.1 Samples**

CD1 mice (Charles River) were used for all experiments. Expression of CSF1R was tested in E13.5, E15.5, and E16.5 mouse embryos, which were received from the Underhill lab at the University of British Columbia. In addition, E18 mouse embryos and P3, P5, P21, and 2-month-old mice were received from the Kurrasch lab at the University of Calgary. All samples were received fixed in 2% or 4% paraformaldehyde (PFA), to preserve tissues.

### **2.2 Experimental design for CSF1R inhibition**

All CSF1R inhibition experiments were conducted in the Kurrasch lab at the University of Calgary. Embryonic CSF1R inhibition was achieved by administering the Plexxikon CSF1R inhibitor drug, PLX5622 (1200 PPM added to chow AIN-76A, Research Diets), to pregnant dams daily from embryonic day 3.5 (E3.5) to birth, which covers gastrulation until full organogenesis has taken place. Control dams received control diet (AIN-76A, Research Diets, New Brunswick, NJ). Considering the role of endometrial macrophages in pregnancy, drug treatment earlier than E3.5 may have interfered with implantation [138]. E18 mouse embryos and P3 and P5 mice exposed to CSF1R inhibition *in utero* were sacrificed. Few mice received postnatal CSF1R inhibition by administering PLX5622 daily for four weeks starting at P28 after weaning. Control mice received control diet. Mice generated from control diet and PLX5622 diet fed dams were put on a wet diet after weaning, to help mice experiencing feeding problems due to craniofacial and/or dental abnormalities.

### **2.3 Tissue preparation**

E13.5, E15.5, and E16.5 CD1 heads, and some E18 control and PLX5622 heads were washed immediately in PBS at 4°C and then stored in 70% ethanol at room temperature until further processing for embedding and sectioning. Some E18 and all P3 and P5 control and PLX5622 heads were decalcified in 14% EDTA pH 7.4 daily for 5 days while shaken at room temperature, and then washed in PBS and stored in 70% ethanol. Some P21 heads were decalcified for 6 days. Samples were automatically processed for further dehydration and clearing in xylene in the Leica Tissue Processor for paraffin embedding. Heads were sectioned sagittally or coronally at 7  $\mu\text{m}$  using an American Optical Microtome. Tissue sections were adhered to super frost plus glass microscope slides. Paraffin sections were used for all histology and immunofluorescence techniques.

### **2.4 Histology**

#### **2.4.1 Hematoxylin and Eosin (H&E) Stain**

Tissues were stained with filtered 50% hematoxylin (Fisher Scientific H-345) in dH<sub>2</sub>O and 1% Eosin Y (B.D.H Stains product 34027) in dH<sub>2</sub>O. Acid alcohol, 1:100 concentrated HCl in 95% ethanol, was used to destain and differentiate hematoxylin. Detailed staining procedure is described in Appendix A.

#### **2.4.2 Von Kossa and MacNeal's Tetrachrome Stain**

This bone stain gives a clear contrast between mineralized tissues and surrounding soft tissues. It cannot be used on decalcified tissues. The original protocol was created for use on plastic embedded samples [139,140]. Bone samples from older mice have high amounts of calcified

tissue and are thus embedded in plastic (e.g. methyl methacrylate) [141]. However, the samples used here were of embryonic ages and did not need plastic embedding. Therefore, the protocol was adapted for undecalcified paraffin embedded samples. E18 control and PLX5622 mouse heads were stained. Silver nitrate stained calcified bone black. Tissues were counterstained with MacNeal's Tetrachrome. Cartilage and nuclei were stained in purple and dark blue, respectively. Detailed staining procedure is described in Appendix B.

### **2.4.3 Pollak's Trichrome Stain**

This stain is an improved method based on Masson's Trichrome stain for distinguishing connective tissue such as collagen from neighbouring cells [142,143]. P3 and P5 control and PLX5622 sections were stained. Collagen stained dark blue green. Nuclei stained in black. Fast green FCF was substituted for light green SF to avoid fading seen with the latter dye. Detailed staining procedure is described in Appendix C.

### **2.5 TRAP Stain**

E18, P3, and P5 control and PLX5622 sections were stained for histochemical localization of TRAP. Tissues were incubated for an hour at 37°C in TRAP staining solution mix and counterstained with fast green. Detailed staining procedure is described in Appendix D.

### **2.6 Immunofluorescence (IF)**

Single or double IF were performed against CSF1R or CSF1R and CSF1, respectively. Primary antibodies used were sheep anti-CSF1R (polyclonal R&D AF3818) and goat anti-CSF1 (polyclonal R&D AF416) at 10 µg/mL. All negative controls were performed with pre-immune

sera from the relevant host animal rather than omitting the primary antibodies, to increase sensitivity of the assays. These included normal sheep IgG (R&D 5-001-A) and normal goat IgG (Vector I-5000) at 10  $\mu\text{g}/\text{mL}$ . Secondary antibodies used were donkey anti-sheep IgG Alexa Fluor 647 (Invitrogen A-21448) and donkey anti-Goat IgG Alexa Fluor 488 (Invitrogen A-11055) at 8  $\mu\text{g}/\text{mL}$ . Detailed staining procedure is described in Appendix E.

## **2.7 Image Scanning**

Slides were scanned with brightfield or fluorescence imaging using an automatic digital slide scanner (3DHISTECH Panoramic MIDI). The exposure time was set at 100 ms and focus frequency was set between 5 and 10 depending on the size of tissues. Fluorescent filter sets used were DAPI, Alexa 488, and Cy5.

## **2.8 Micro-computed Tomography (Micro-CT)**

P21 and 2-month-old mice were set in falcon tubes with 0.5% agarose. High-resolution micro-CT imaging was performed at the Center for High Throughput Phenogenomics at the University of British Columbia using a Scanco Medical  $\mu\text{CT}100$  scanner at 55 kVp, 200  $\mu\text{A}$  with an isometric resolution of 34.4  $\mu$ . The scanned images were rendered using 3D slicer. Teeth were segmented using manual and semi-automated segmentation tools based on thresholding. Segmented areas were converted into models for visualization. To view internal structures such as the cervical loop regions, clipping planes were placed in homologous areas between experimental and control scans.

## Chapter 3: Results

### 3.1 CSF1 receptor and ligand expression during odontogenesis

While a few studies have found expression of CSF1R transcripts or protein in postnatal dental tissues in rodent models, nothing is known about its expression during early odontogenesis [22,89]. Therefore, anti-CSF1R antibody was used in embryonic mouse tissues to determine the spatial and temporal odontogenic expression of CSF1R protein, mainly in the developing incisors.

Immunostaining of CSF1R in mouse mandibular and maxillary tissues showed age-specific differences during odontogenesis. At E13.5, CSF1R was primarily absent in the incisor bud (Figure 3.1A). At E15.5 and onwards, the number of CSF1R-stained cells increased with the developmental progression of teeth. At E15.5 and E16.5, the ectomesenchyme directly encompassing the OEE in incisor caps stained for CSF1R<sup>+</sup> cells (Figure 3.1A, B; arrowheads). At E16.5, the dental papilla stained for CSF1R (Figure 3.1B). At E18, CSF1R<sup>+</sup> cells were similarly located around the ectomesenchyme surrounding the incisor's bell-shaped enamel organs (Figure 3.1B; Figure 3.2A). The number of CSF1R<sup>+</sup> cells was greater at the apical (proximal or posterior) end of the mandibular incisor germ, more along the labial and lingual dental epithelium, around the cervical loops than the distal ectomesenchyme (Figure 3.2A, A', A"). Although the number of CSF1R-expressing cells in the proximal region around the mandibular incisor germ appeared uniformly strong, there were fewer positive cells around the maxillary incisor germ. Notably, the number of positive cells aboral to the labial dental epithelium was higher than that oral to the lingual dental epithelium in E18 maxillary incisors (Figure 3.1B). Double IF was performed in E18 mandibular incisor germs using anti-CSF1R

and anti-CSF1 antibodies. CSF1 ligand had a similar expression pattern as its cognate receptor in the ectomesenchyme and strongly colocalized with CSF1R on the same ectomesenchymal cells surrounding the incisor bell (Figure 3.2B, B', B''). This colocalization was stronger in the area proximal to the cervical loops (Figure 3.2B'). Both CSF1R and CSF1 were faintly stained in the dental papilla (Figure 3.1B; Figure 3.2A, B).

The immunostaining pattern of CSF1R in molar germs studied at E18 was similar to that seen in incisors (Figure 3.3). The ectomesenchyme surrounding the OEE of the molar germ contained cells expressing CSF1R. At E18, intensity was highest in the aboral and mesial tissues. Some faint staining was found in the dental papilla. Notably, at all embryonic time points there was no immunostaining of CSF1R in the incisor and molar dental epithelial tissues, which include the OEE, IEE, stellate reticulum, stratum intermedium, and cervical loops.

To confirm previous reports of CSF1R expression in postnatal dental tissues, immunostaining was performed in mandibular tissues at P3 and P5. The patterns of CSF1R expression found in the ectomesenchyme around developing incisors at these ages resembled that of the E18 incisor germ (Figure 3.1A). Immunostaining was present in the distal region of the dental pulp but absent in the ameloblasts and odontoblasts (Figure 3.1A; Appendix F). The patterns of CSF1R expression in the ectomesenchyme around developing molars at P3 and P5 resembled that of the E18 molar germ (Figure 3.3). The second molar germs had CSF1R immunostaining in the aboral and distal ectomesenchyme cells. Faint staining was present in the molar dental papilla postnatally. However, similar to incisors, there was no staining for the receptor in the specialized dental cells, the ameloblasts and odontoblasts.

For our IF experiments, we performed negative control tests, in which pre-immune normal sheep IgG was used as the primary antibody instead of anti-CSF1R antibody. We detected no immunostaining in or around developing teeth at all embryonic and postnatal time points. E15.5 and E18 pre-immune normal sheep IgG controls are shown (Figure 3.1; Figure 3.2; Figure 3.3). In negative controls where pre-immune normal goat IgG was used as the primary antibody instead of anti-CSF1 antibody, some autofluorescence in tissues outside the developing teeth and faintly in the dental papilla was detected at all times. E18 pre-immune normal goat IgG control is shown (Figure 3.2). The autofluorescent cells were most probably red blood cells since they had biconcave disk shapes. Red blood cells have overlapping excitation and emission spectra with green-fluorescent reporters [144]. In addition, blood vessels are reported to form during odontogenesis around tooth germs, which migrate into the dental papilla and reside there in the future dental pulp [145]. Accordingly, clusters of cells in the ectomesenchyme and dental papilla that stained with anti-CSF1 antibody were considered background due to red blood cells (Figure 3.2).

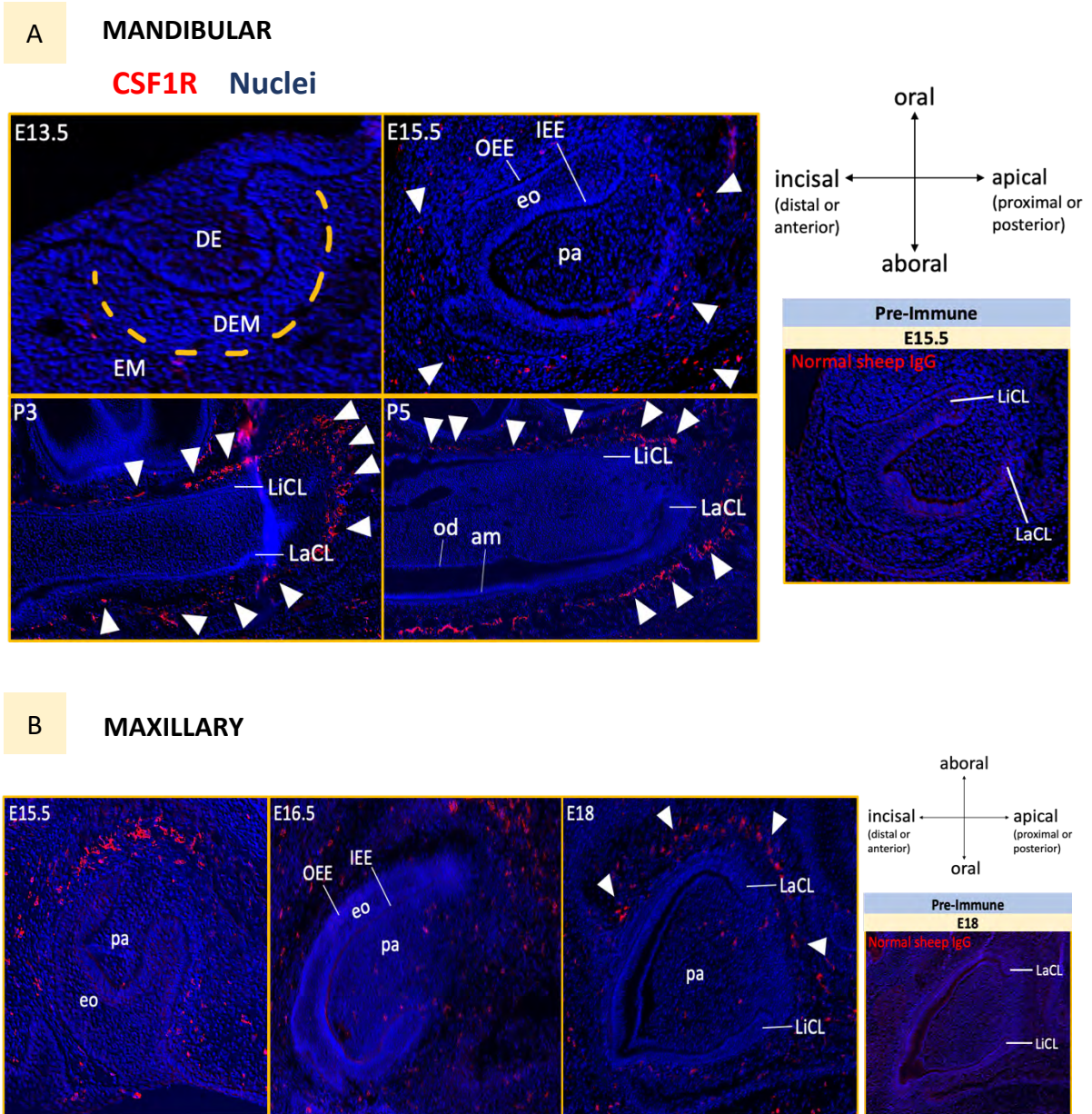


**Figure 3.1. CSF1R expression in odontogenesis.** CSF1R and nuclei in red (arrowheads) and blue, respectively. (A) Mandibular incisor germs at E13.5 (condensing dental ectomesenchyme is outlined in yellow lines), E15.5, P3, and P5. Pre-immune negative control at E15.5 on right. (B) Maxillary incisor germs at E15.5, E16.5, and E18. Pre-immune negative control at E18 on right.  $n = 2$  to  $3$  at each age. Ameloblasts (am), dental epithelium (DE), dental ectomesenchyme (DEM), dental papilla (pa), ectomesenchyme (EM), enamel organ (eo), inner enamel epithelium (IEE), labial cervical loop (LaCL), lingual cervical loop (LiCL), odontoblasts (od), outer enamel epithelium (OEE).

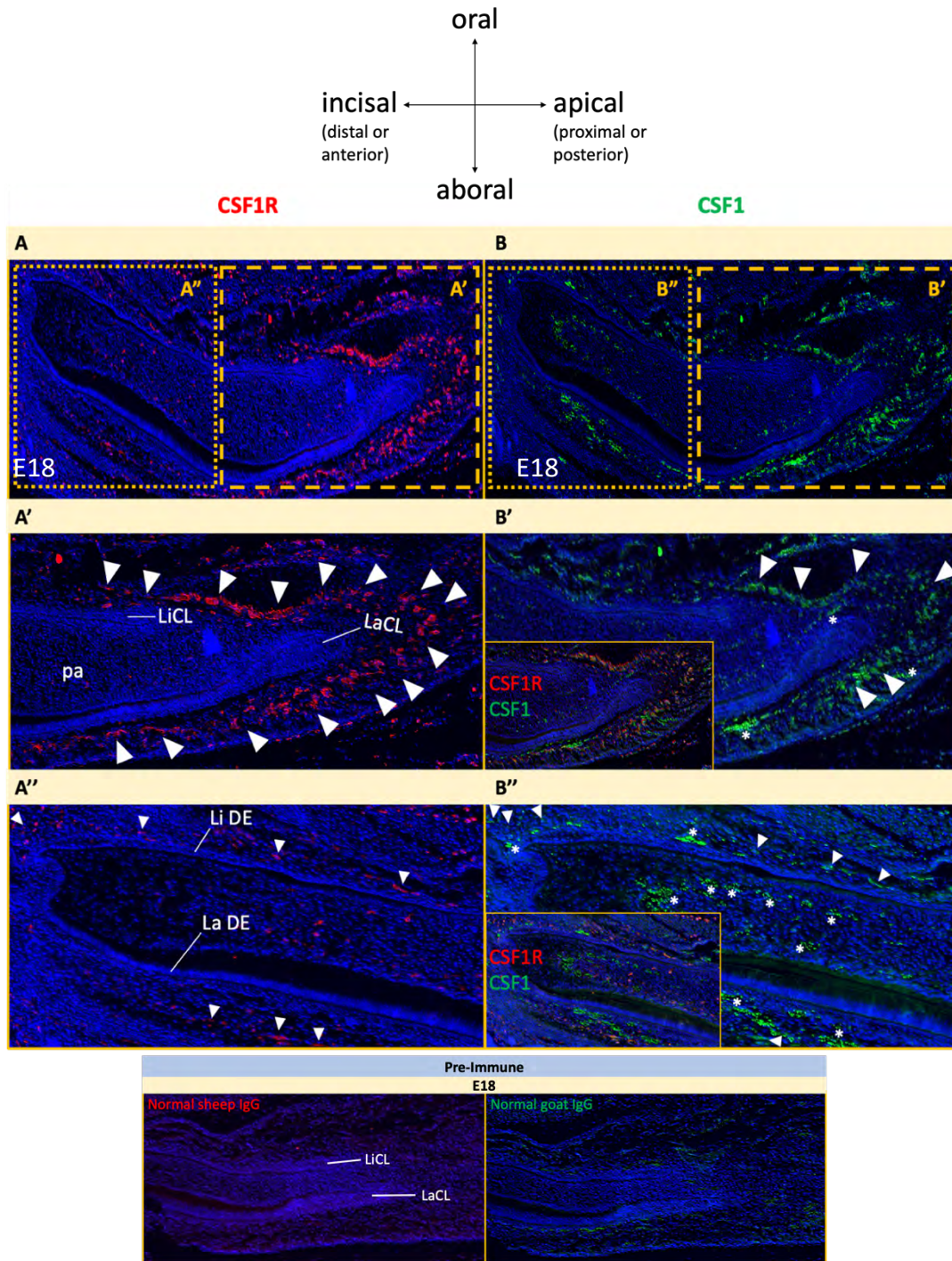


**Figure 3.2. CSF1/CSF1R expression in the E18 mandibular incisor.** CSF1R and CSF1 in red and green, respectively (arrowheads). Nuclei in blue. (A') Apical or proximal end, (A'') distal end of incisor from A. (B') Apical or proximal end, (B'') distal end of incisor from B. (Inset in B') CSF1/CSF1R double immunostaining. Autofluorescent blood cells are marked by asterisks (\*). Pre-immune negative controls at E18 on bottom.  $n = 3$ . *Dental papilla (dp)*, *labial cervical loop (LaCL)*, *labial dental epithelium (La DE)*, *lingual cervical loop (LiCL)*, *lingual dental epithelium (Li DE)*.

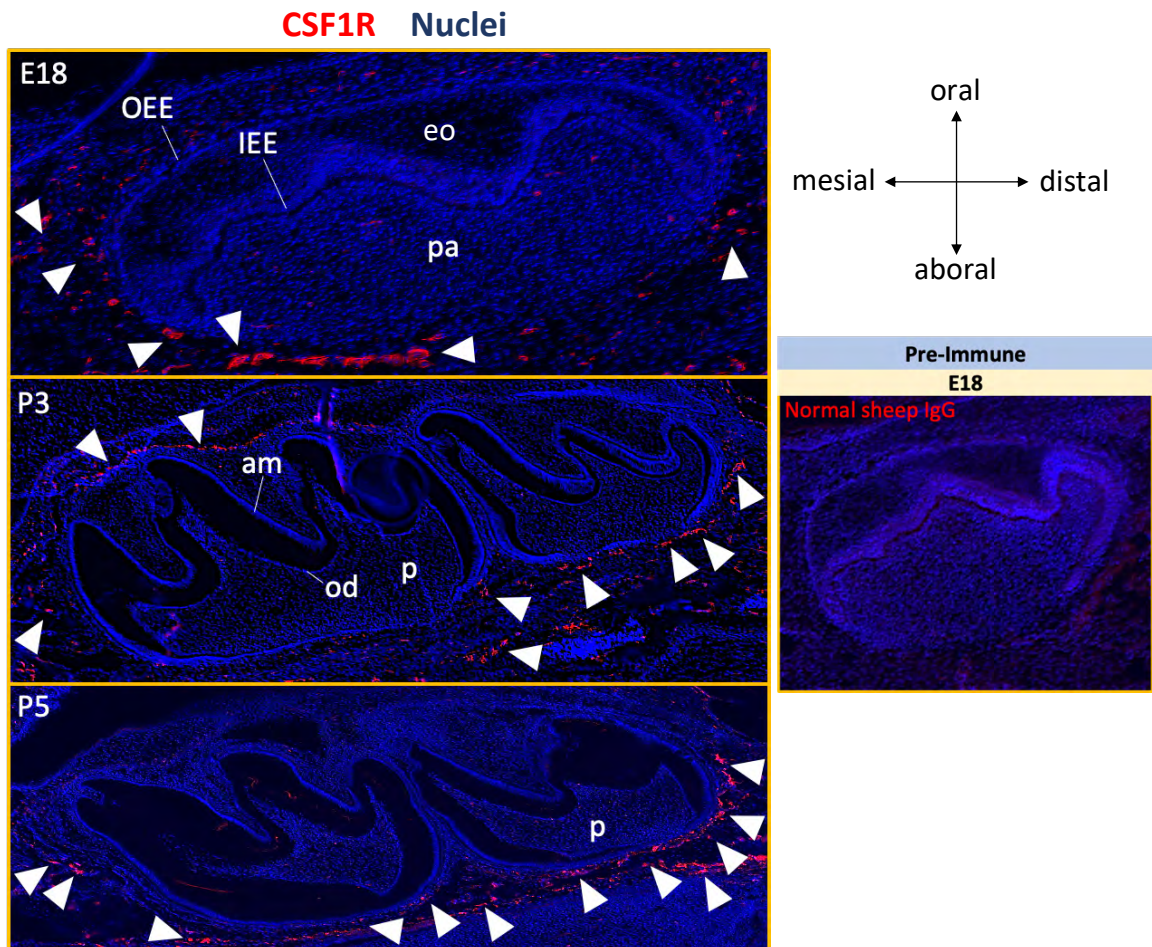


**Figure 3.3. CSF1R expression in mandibular molars at E18, P3, and P5.** CSF1R and nuclei in red (arrowheads) and blue, respectively. Pre-immune negative control at E18 on right.  $n = 3$  at each age. Ameloblasts (*am*), dental papilla (*pa*), enamel organ (*eo*), inner enamel epithelium (*IEE*), odontoblasts (*od*), outer enamel epithelium (*OEE*), pulp (*p*).

### 3.2 Phenotype analysis of embryonic CSF1R inhibition in developing teeth

Given the abundant expression of CSF1R expression detected around developing dental tissues, we wished to examine its role in odontogenesis. Although dental abnormalities have been associated with tooth eruption failure in *Csf1<sup>op/op</sup>* mice, they have not well described. With regards to receptor null mice (*Csf1r<sup>-/-</sup>*), tooth abnormalities have not been studied at all (see 1.3.2). Hence, is unknown if lack of normal CSF1 or CSF1R affects early odontogenesis or strictly the tooth eruption process. In a previous study done by our lab, dental abnormalities were analyzed more carefully in adolescent mice using a CSF1R inhibitor [23]. The pharmacological model using the CSF1R inhibitor-PLX5622, was again employed here during the embryonic stages of odontogenesis for further phenotype analysis in developing teeth at prenatal and postnatal times (Figure 3.4).

Briefly, PLX6522 was administered to pregnant dams between E3.5 and E18. At E18, CSF1R immunostaining could not be detected in mice exposed to PLX5622 *in utero*, thus indicating the specificity of PLX5622 for CSF1R (Figure 3.5). Dental abnormalities were observed at E18 in the mandibular and maxillary incisors of CSF1R-inhibited mice (Figure 3.6B, D; Figure 3.7B, D) in comparison to controls (Figure 3.6A, C; Figure 3.7A, C). In treated mice, H&E staining of incisors revealed notching or infoldings in the dental epithelium near the labial cervical loops (Figure 3.6B). Ameloblasts and odontoblasts maintained their normal columnar shapes and polarities, except at the regions of infoldings where they appeared flat (Figure 3.6B'; Figure 3.7B'). In controls, the Von Kossa technique with tetrachrome counterstain revealed mineralized bone developing neatly around incisor germs (Figure 3.6C; Figure 3.7C). Distinct soft tissue spaces containing the DF, likely the tooth-bone interfaces (TBI), were noted

between the incisor germs and bone [146]. In contrast, these spaces in CSF1R-inhibited mice were clearly thinner on the distal side and absent on the apical side of incisor germs, with a concomitant increased presence of bone (Figure 3.6D; Figure 3.7D). The OEE in locations within and near the labial dental epithelial infoldings made direct contact with the neighbouring bone in certain spots, which appeared more prominent in the maxilla (Figure 3.6D; Figure 3.7D). Meckel's cartilage in the mandibles of CSF1R-inhibited mice (Figure 3.6D') was more mineralized than in controls (Figure 3.6C'). Areas of agglomerated nuclei, possibly osteoclasts, were seen between the apical ends of the mandibular incisor germs and distal (anterior) ends of Meckel's cartilage, on the lateral (buccal) surfaces of Meckel's cartilage, and around the maxillary incisor germs in control mice but not in treated mice (Figure 3.6C'; Figure 3.7C'). In controls, the lacunae on more distal ends of Meckel's cartilage were degraded (Figure 3.6C') but were intact in treated mice (Figure 3.6D'). Similar results were noted when viewing sections in the coronal plane in mandibular incisors in treated mice. There was greater bone mineralization between dental epithelium and the buccal surfaces of Meckel's cartilage and an absence of areas with multinucleated cells (Figure 3.8B) when compared with controls (Figure 3.8A).

Notably, dental abnormalities were present postnatally in incisors at P3, P5, and P21 despite the withdrawal of PLX5622 at birth. At P3, the cervical loops of mandibular incisor germs in control mice were located beneath (aboral to) and just posterior to first molars (Figure 3.9A). Ectomesenchymal sacs containing the DF separated incisor germs from the surrounding bone (Figure 3.9C). However, in CSF1R-inhibited mice, cervical loops were poorly defined, and the dental epithelium failed to reach the level of the first molars (3.9B). Apical ends of the incisor

germs were interrupted by surrounding bone, causing the ameloblasts, odontoblasts, and dental ectomesenchymal cells of the dental pulp to branch and entwine with the bone trabeculae (Figure 3.9B', D). At P5, dental epithelium of mandibular incisor germs in control mice had elongated to positions below the second molars (Figure 3.9E). In parallel, the surrounding bone still maintained distance from the developing incisors with a well-defined TBI (Figure 3.9G). By contrast in CSF1R-inhibited mice, cervical loops were abnormal, and the dental epithelium remained in similar positions seen at P3 and appeared to be stalled anterior to the first molar (Figure 3.9B, F). Incisor germ epithelium was closely surrounded by bone, which had encroached into the dental follicular spaces. Branches of dental cells within the bone still appeared at the apical ends at P5 (Figure 3.9H).

At P3 and P5, maxillary incisor germs appeared drastically more malformed than mandibular incisor germs in CSF1R-inhibited mice. The normal curved and crescentic morphologies of maxillary incisors at E18, P3, and P5 (Figure 3.7A; Figure 3.10A; Figure 3.11A) had disappeared, and the labial dental epithelium was not positioned as high, aborally and proximally, in the maxilla (Figure 3.10B; Figure 3.11B). Cervical loops were interrupted, and branches of ameloblasts, odontoblasts, and dental ectomesenchymal cells formed off the labial surfaces (Figure 3.10B'; Figure 3.11B'). Surrounding bone trabeculae converged around the apical ends of the incisor germs and came into contact with the labial and lingual dental epithelial surfaces, especially the ameloblasts on the labial surfaces (Figure 3.10D; Figure 3.11D). The normal ectomesenchymal TBI space around the incisor germs had been invaded by the bone in CSF1R-inhibited mice (Figure 3.10C, D; Figure 3.11C, D). However, at P5, the distance between dental ectomesenchymal cells in the most apical ends of maxillary incisor

germs and the surrounding bone in CSF1R-inhibited mice had rather increased so that the bone was no longer in contact with the dental pulp (Figure 3.11D). The normal polarities and shapes of ameloblasts and odontoblasts were maintained in both the mandibular and maxillary incisor germs at P3 and P5 but were flattened at the interrupted apical ends (Figure 3.9A', B', E', F'; Figure 3.10A'', B''; Figure 3.11A', B').

Mandibular first molars were observed sagittally and coronally at E18 and P5. Sagittally, the enamel organs in CSF1R-inhibited mice appeared thinner than in controls, whereas ameloblasts and odontoblasts were normal (Figure 3.12A, B, E, E', F, F'). Type 1 collagen, the organic matrix of bone, was stained using the Pollak's trichrome method to visualize the development of connective tissue around molars at E18. Compared to controls (Figure 3.12C), bone anterior and aboral to the molar germs were closer to their mesial and apical surfaces, respectively, although it was more evident on the mesial surfaces (Figure 3.12D). The tissue spaces containing the DF between the molar germs and bone was also thinner (Figure 3.12D). Coronally, molar germs in CSF1R-inhibited mice appeared narrower in the buccal-lingual axis and had thinner enamel organs (Figure 3.13B) than in control mice at E18 (Figure 3.13A). Control molar germs were developing in mineralized bony crypts and had well-spaced boundaries separating them from the bone (Figure 3.13A, C), whereas in treated mice these boundaries were nearly lost (Figure 3.13B, D). As a result, the bone had almost encroached into the OEE buccally near the cervical loop (Figure 3.13D). At P5, no differences in ameloblasts and odontoblasts were found between control and treated mice (Figure 3.12E', F').

At P21, micro-CT and histology methods were used to show that dental abnormalities from PLX5622 exposure persisted due to embryonic perturbations. In controls, labial cervical loops of mandibular incisors were positioned just proximal to the level of the third molar distal surfaces, as expected (Figure 3.14A). In CSF1R-inhibited mice, the cervical loops were difficult to discern and failed to grow past the third molars, since they were positioned distal to the first molars (Figure 3.14B). CSF1R-inhibited mice also displayed variability in presentation of their maxillary and mandibular incisors. The maxillary incisors appeared branched or geminated, showing single ectopic tooth structures of smaller size fused to the labial surface of the original incisors (Figure 3.15A, B2). The mandibular incisors had irregular infoldings in the dentin-enamel junction and disorganized pulp (Figure 3.15B4). The ameloblasts and odontoblasts maintained their normal columnar shapes and polarities except at the regions of infoldings, where the cells were flattened (Figure 3.15B4).

The numbers of control and PLX5622-treated mice tested and the dental phenotypes displayed in the latter are summarized in Table 1.1.

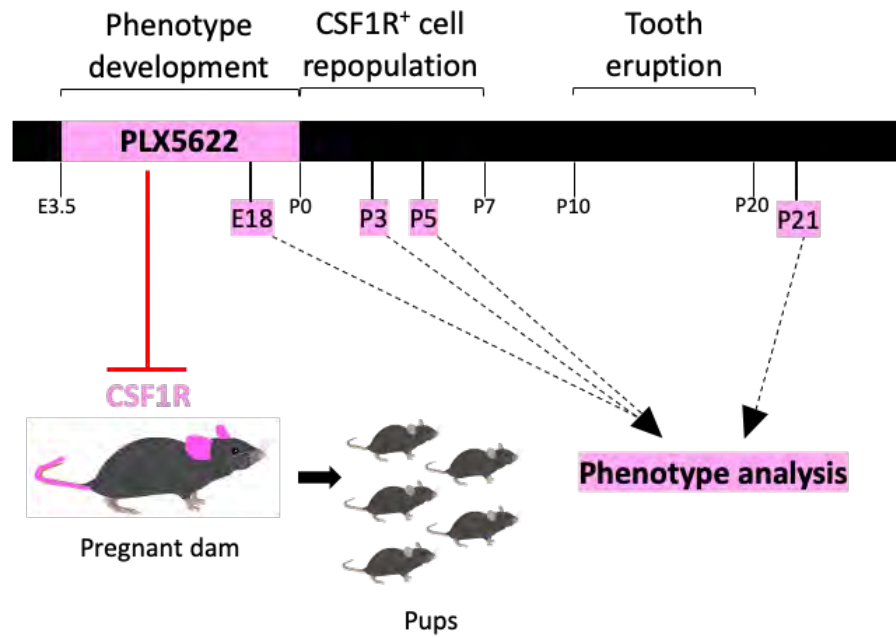


**Figure 3.4. Experimental design.** Pregnant dams received CSF1R inhibitor PLX5622 diet or control diet from E3.5 to birth (P0). Incisors and first molars erupted between P10 and P20. Teeth in mice exposed to PLX5622 treatment *in utero* were assessed at different times (pink highlights). Adapted from [23].

### CSF1R Nuclei

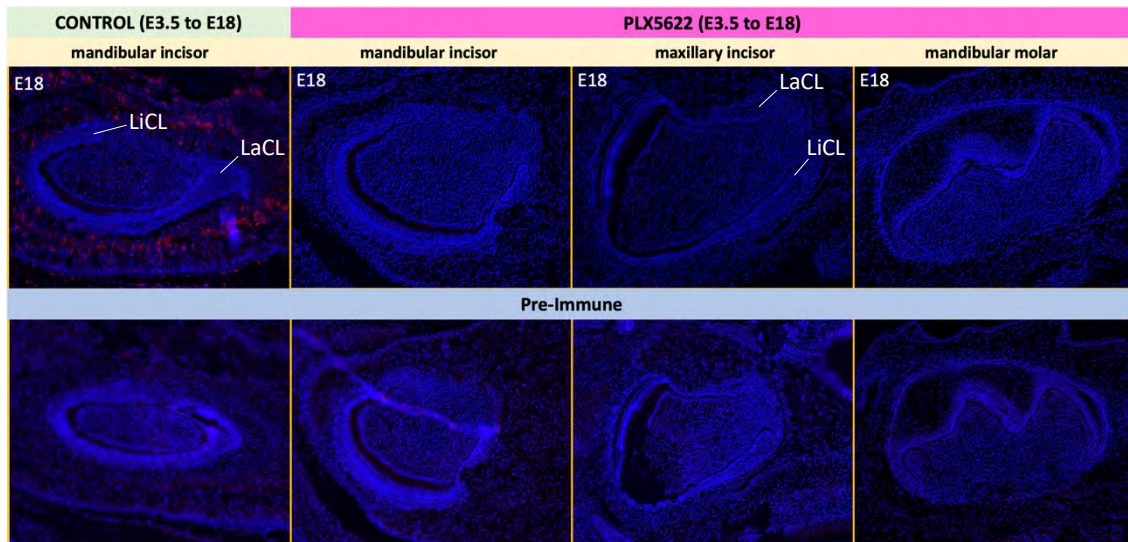


**Figure 3.5. PLX5622 robustness.** Top row: CSF1R immunostaining in mice exposed to control (left column) or PLX5622 (right columns) diet between E3.5 and E18. No CSF1R<sup>+</sup> cells are detected around PLX5622-tooth germs at E18. Bottom row: pre-immune negative controls of control (left column) and PLX5622 (right columns) tooth germs at E18. *Labial cervical loop (LaCL)*, *lingual cervical loop (LiCL)*.

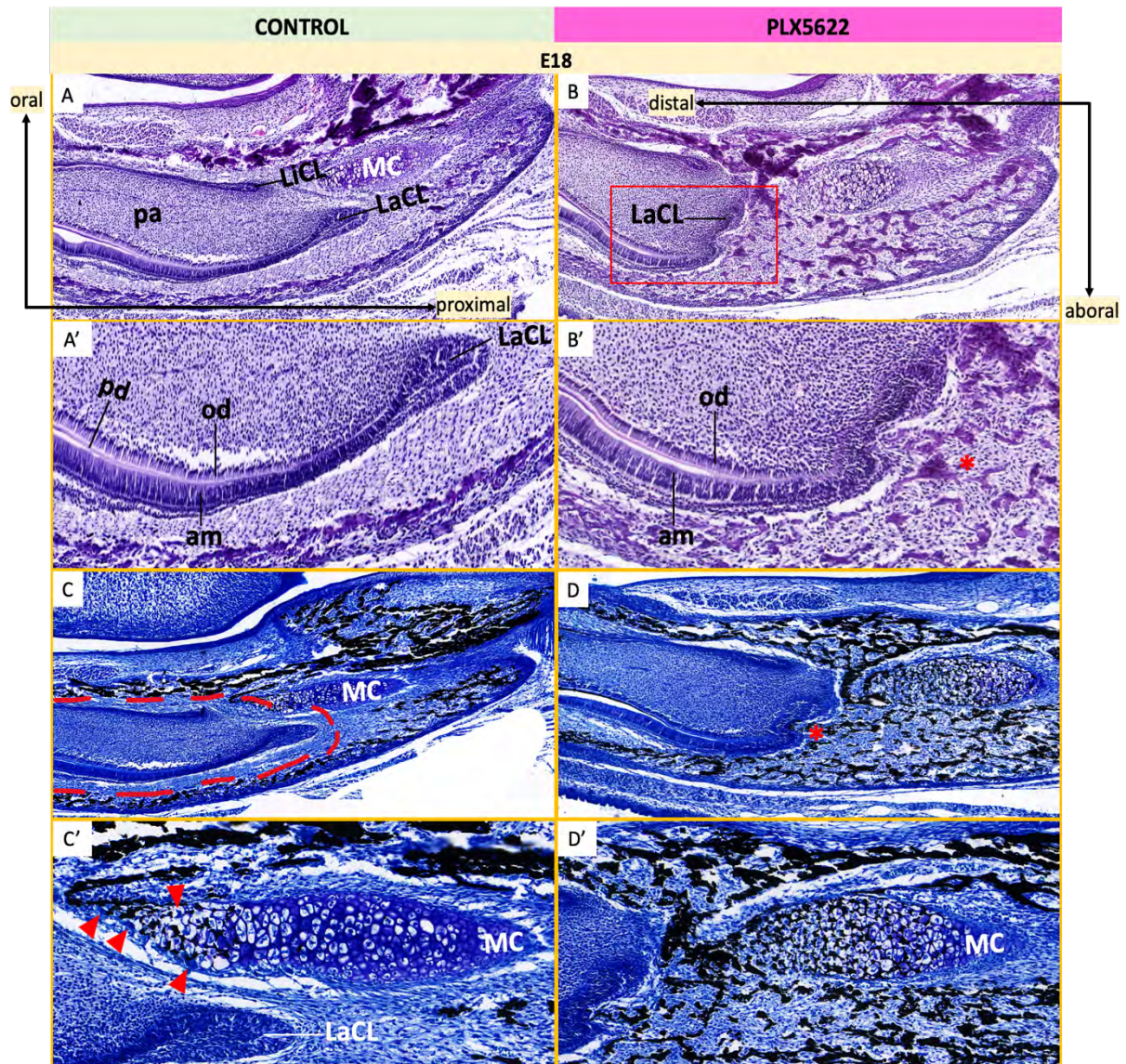


**Figure 3.6. Histological analysis of mandibular incisors at E18.** Left: Tooth germs in control mice stained with (A, A') H&E and (C, C') Von Kossa with tetrachrome counterstain. Right: Tooth germs in mice exposed to CSF1R inhibition with PLX5622 *in utero* stained with (B, B') H&E and (D, D') Von Kossa/tetrachrome. (A') Labial portion of incisor, including the labial cervical loop, from A. (B') Labial portion of incisor, including the labial cervical loop, from B (box). Infolding of odontogenic tissues near labial cervical loop (\*). (D) Mineralized alveolar bone trabeculae (black) bombards the developing incisor (\*). Soft tissue space (C; red lines) between incisor and bone is nearly absent. (C') Proximal portion of mandible from C. Meckel's cartilage is degraded on its lateral surface by multinucleated giant cells (arrowheads). (D') Proximal portion of mandible from D. Meckel's cartilage is heavily mineralized.  $n = 3$  to 5 control and PLX5622-treated mice. Ameloblasts (am), dental papilla (pa), labial cervical loop (LaCL), lingual cervical loop (LiCL), Meckel's cartilage (MC), odontoblasts (od), predentin (pd).

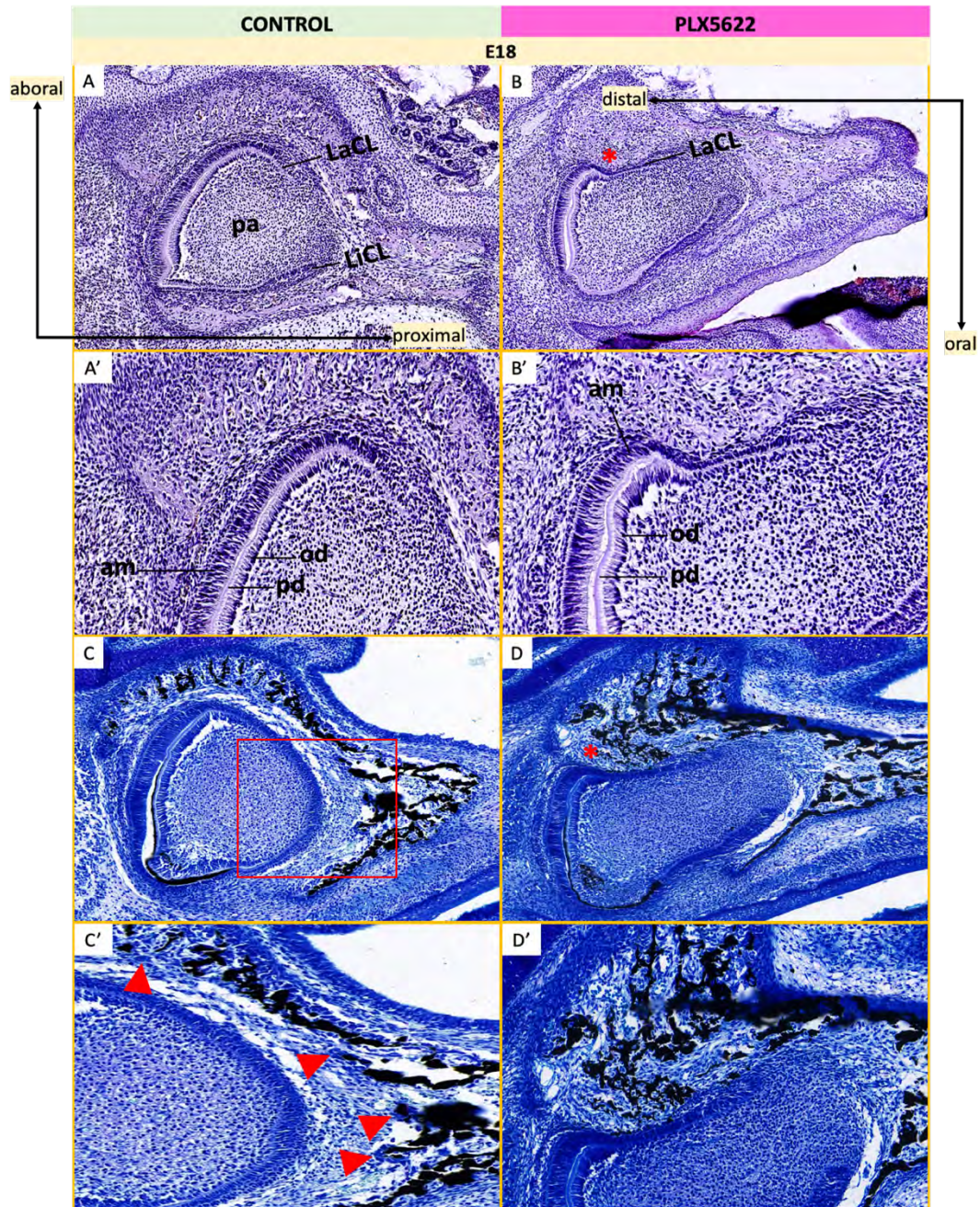


**Figure 3.7. Histological analysis of maxillary incisors at E18.** Left: Tooth germs in control mice stained with (A, A') H&E and (C, C') Von Kossa/tetrachrome. Right: Tooth germs in mice exposed to CSF1R inhibition with PLX5622 *in utero* stained with (B, B') H&E and (D, D') Von Kossa with tetrachrome. (A') Labial portion of incisor, including the labial cervical loop, from A. (B') Labial portion of incisor, including the labial cervical loop, from B. Extreme infolding of odontogenic tissues near labial cervical loop (\*). (D) Mineralized alveolar bone trabeculae (black) bombards the developing incisor, especially at the labial surface (\*). Soft tissue space between incisor and bone is nearly absent. (C') Proximal portion of incisor from C (box). Multinucleated giant cells (arrowheads) line the outer surface of bone. None are found in D'. *n* = 3 to 5 control and PLX5622-treated mice. Ameloblasts (am), dental papilla (pa), labial cervical loop (LaCL), lingual cervical loop (LiCL), odontoblasts (od), predentin (pd).

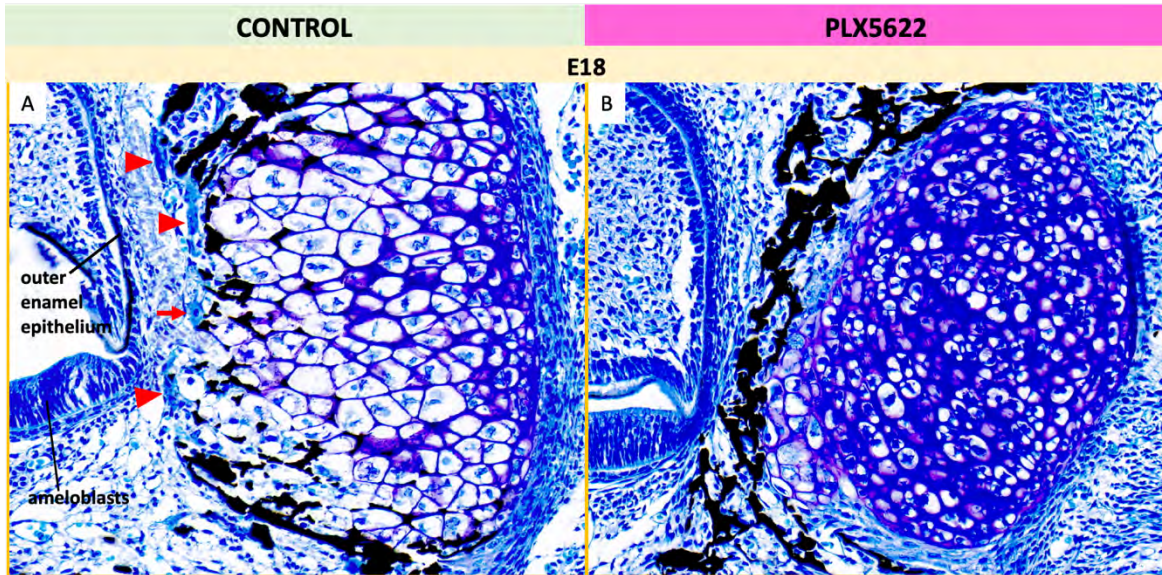
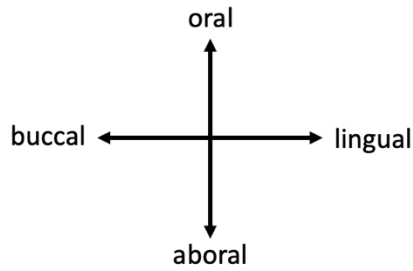


**Figure 3.8.** Meckel's cartilage at E18 stained with Von Kossa/tetrachrome. Coronal sections. Mandibular incisor germ forms lateral or buccal to hypertrophic Meckel's cartilage. (A) In controls, degradation of Meckel's cartilage occurs on the mineralized (black) lateral surface nearest to the incisor germ by multinucleated giant cells (arrowheads). A large macrophage with a single nucleus (arrow) is also seen. (B) No degradation of Meckel's cartilage. There is heavier mineralization between the incisor germ and Meckel's cartilage. *n* = 2 control and PLX5622-treated mice

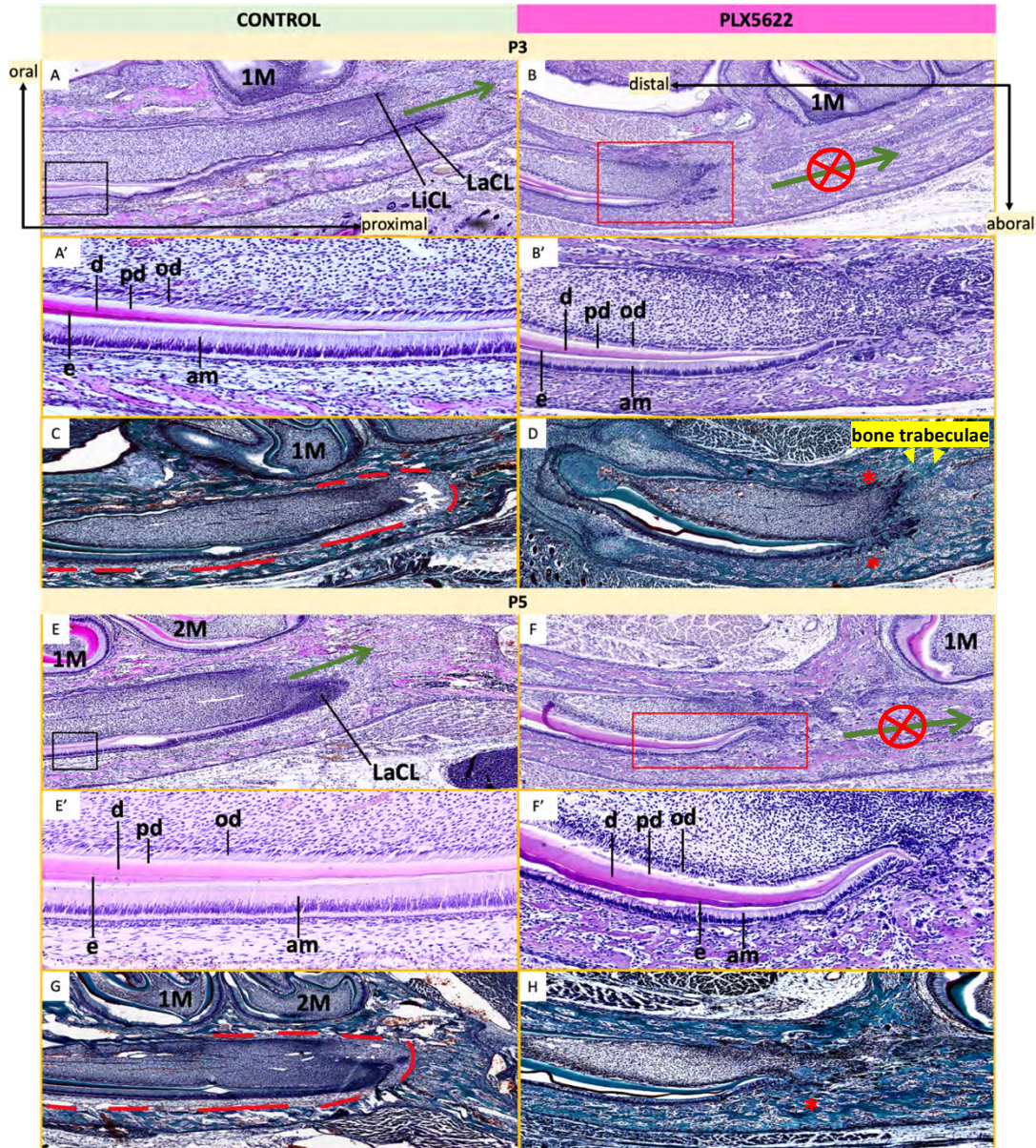


**Figure 3.9. Postnatal histological analysis of mandibular incisors.** Left: Tooth germs in control mice stained with (A, A', E, E') H&E and (C, G) Pollak's trichrome. Right: Tooth germs in mice exposed to CSF1R inhibition with PLX5622 *in utero* stained with (B, B', F, F') H&E and (D, H) Pollak's trichrome. (A) At P3, cervical loops pass the level of the first molar (arrow). (B) At P3, dental epithelium fails to elongate ("X" through arrow) and remains distal to first molar. No cervical loops seen. (B') Apical end of incisor germ from B (box) is fragmented. (E) At P5, cervical loops are at the level of the second molar (arrow). (F) At P5, dental epithelium remains distal to first molar ("X" through arrow). No cervical loops seen. (F') Apical end of incisor germ from F (box) is fragmented. (C, G) At P3 and P5, soft tissue space (red lines) separates the developing incisor from surrounding bone (greenish blue). (D, H) At P3 and P5, bone trabeculae (yellow arrowheads) have taken over the soft tissue space and contact the developing incisor (\*). *n* = 3 to 4 control and PLX5622-treated mice at each age. Ameloblasts (am), dentin (d), enamel (e), first molar (1M), second molar (2M), labial cervical loop (LaCL), lingual cervical loop (LiCL), odontoblasts (od), predentin (pd).

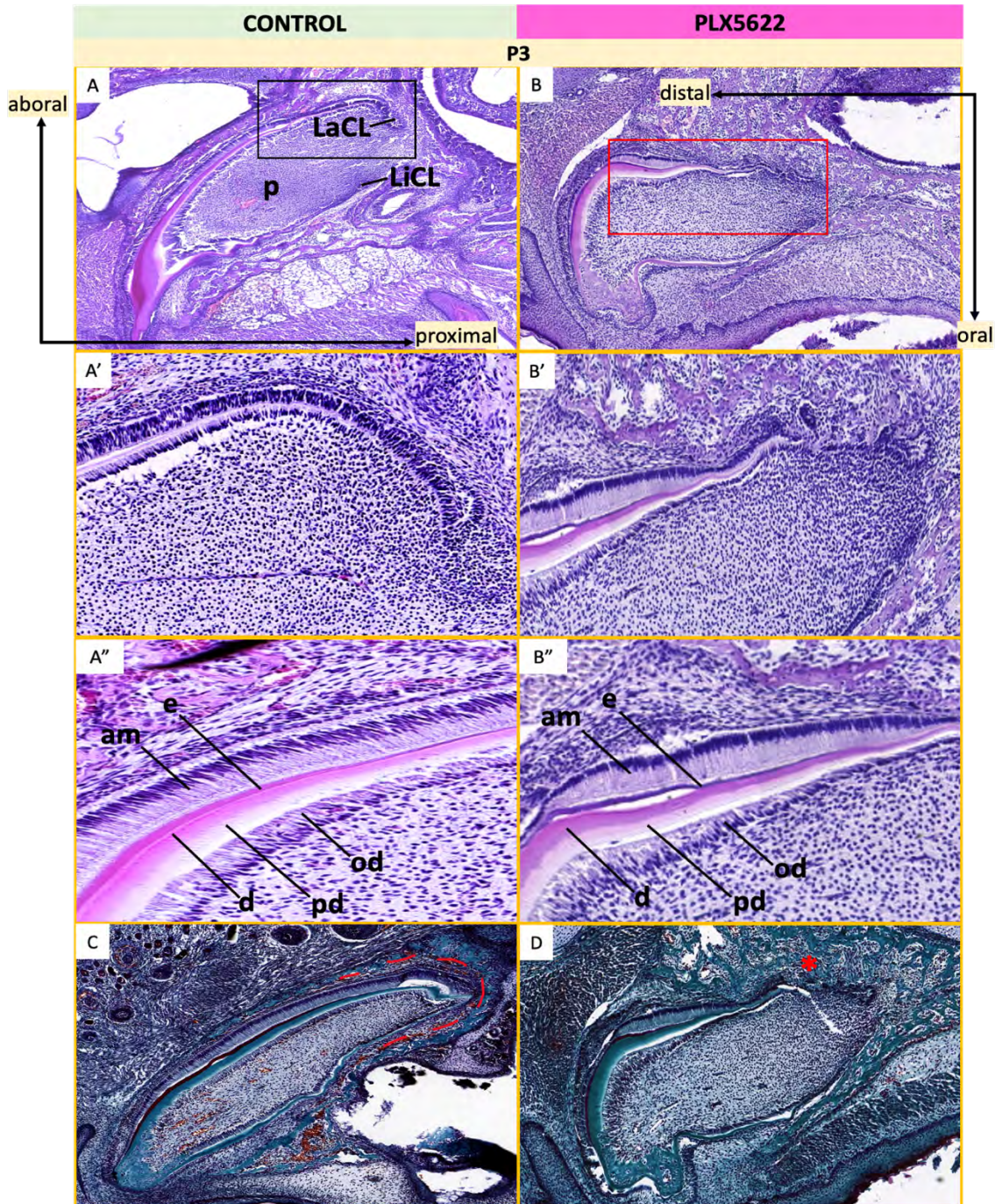


**Figure 3.10. Histological analysis of maxillary incisors at P3.** Left: Tooth germs in control mice stained with (A, A', A'') H&E and (C) Pollak's trichrome. Right: Tooth germs in mice exposed to CSF1R inhibition with PLX5622 *in utero* stained with (B, B', B'') H&E and (D) Pollak's trichrome. (B) Altered morphology. (B') Labial surface from B (box) is fragmented on apical end, in comparison to labial surface of A'. (A'', B'') Dental cells are normal except in regions of fragmentation. (D) Surrounding tissue/bone (greenish blue) in complete contact with incisor germ (\*), in comparison to C (red lines). *n* = 3 to 4 control and PLX5622-treated mice. Ameloblasts (am), dentin (d), enamel (e), labial cervical loop (LaCL), lingual cervical loop (LiCL), odontoblasts (od), predentin (pd), pulp (p).

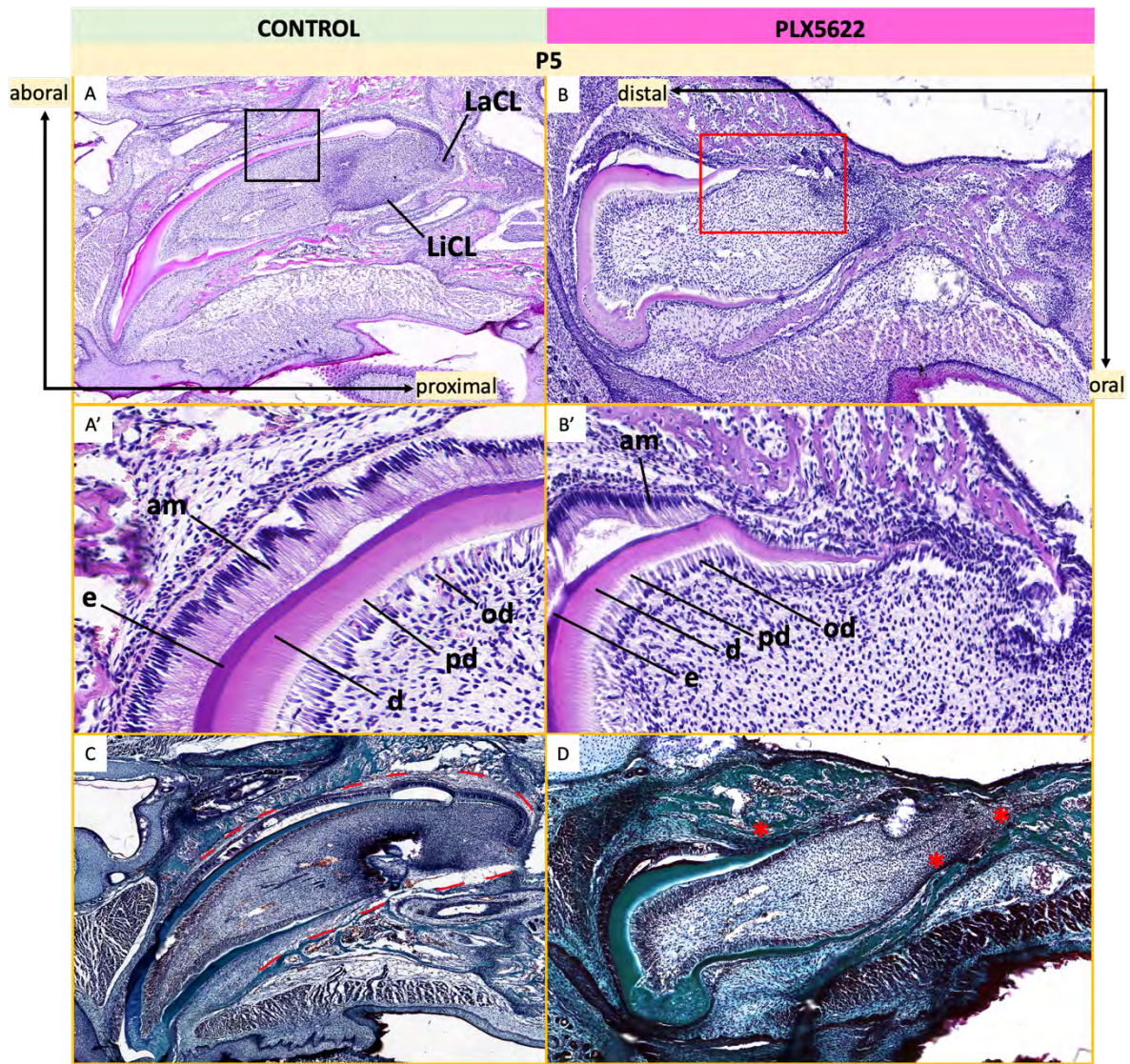


**Figure 3.11. Histological analysis of maxillary incisors at P5.** Left: Tooth germs in control mice stained with (A, A') H&E and (C) Pollak's trichrome. Right: Tooth germs in mice exposed to CSF1R inhibition with PLX5622 *in utero* stained with (B, B') H&E and (D) Pollak's trichrome. (B) Altered morphology, in comparison to A. (B') Labial surface from B (box) is fragmented on apical end, in comparison to labial surface of A'. (A', B') Dental cells are normal except in regions of fragmentation. (D) Surrounding tissue/bone (greenish blue) in complete contact with incisor germ (\*), in comparison to C (red lines). *n* = 3 control and PLX5622-treated mice. Ameloblasts (am), dentin (d), enamel (e), labial cervical loop (LaCL), lingual cervical loop (LiCL), odontoblasts (od), predentin (pd).

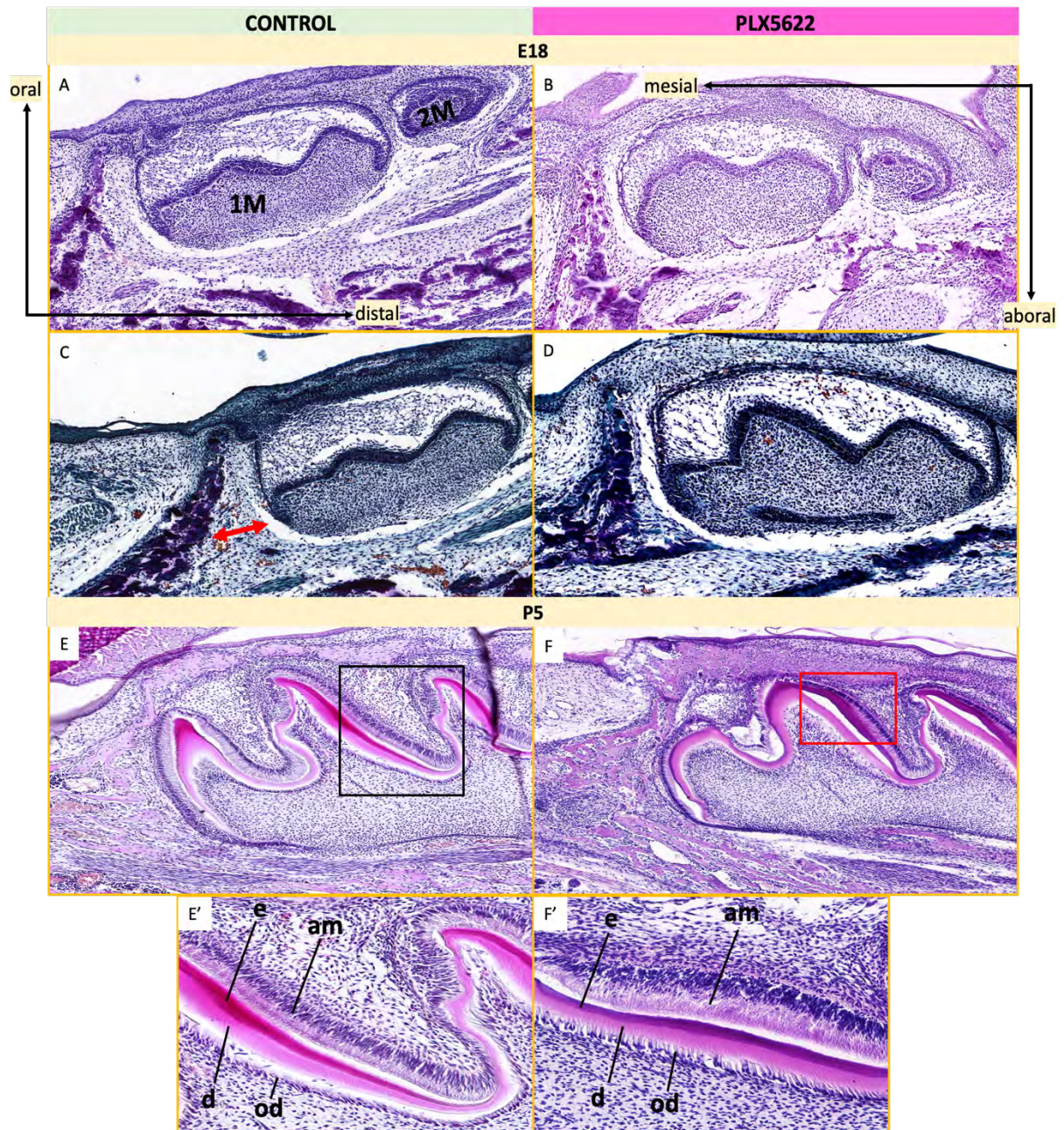


**Figure 3.12. Histological analysis of mandibular first molars at E18 and P5.** Left: Tooth germs in control mice stained with (A, E, E') H&E and (C) Pollak's trichrome. Right: Tooth germs in mice exposed to CSF1R inhibition with PLX5622 *in utero* stained with (B, F, F') H&E and (D) Pollak's trichrome. (B, F') At E18 and P5, enamel organs appear thinner, in comparison to controls A and E, respectively. (C) A clear space (double arrow) separates the molar germ from bone (purple). (D) Bone is in closer proximity to molar germ on its distal side. (E', F') Dental cells are normal.  $n = 3$  to 5 control and PLX5622-treated mice at each age. Ameloblasts (am), dentin (d), enamel (e), first molar (1M), odontoblasts (od), second molar (2M).

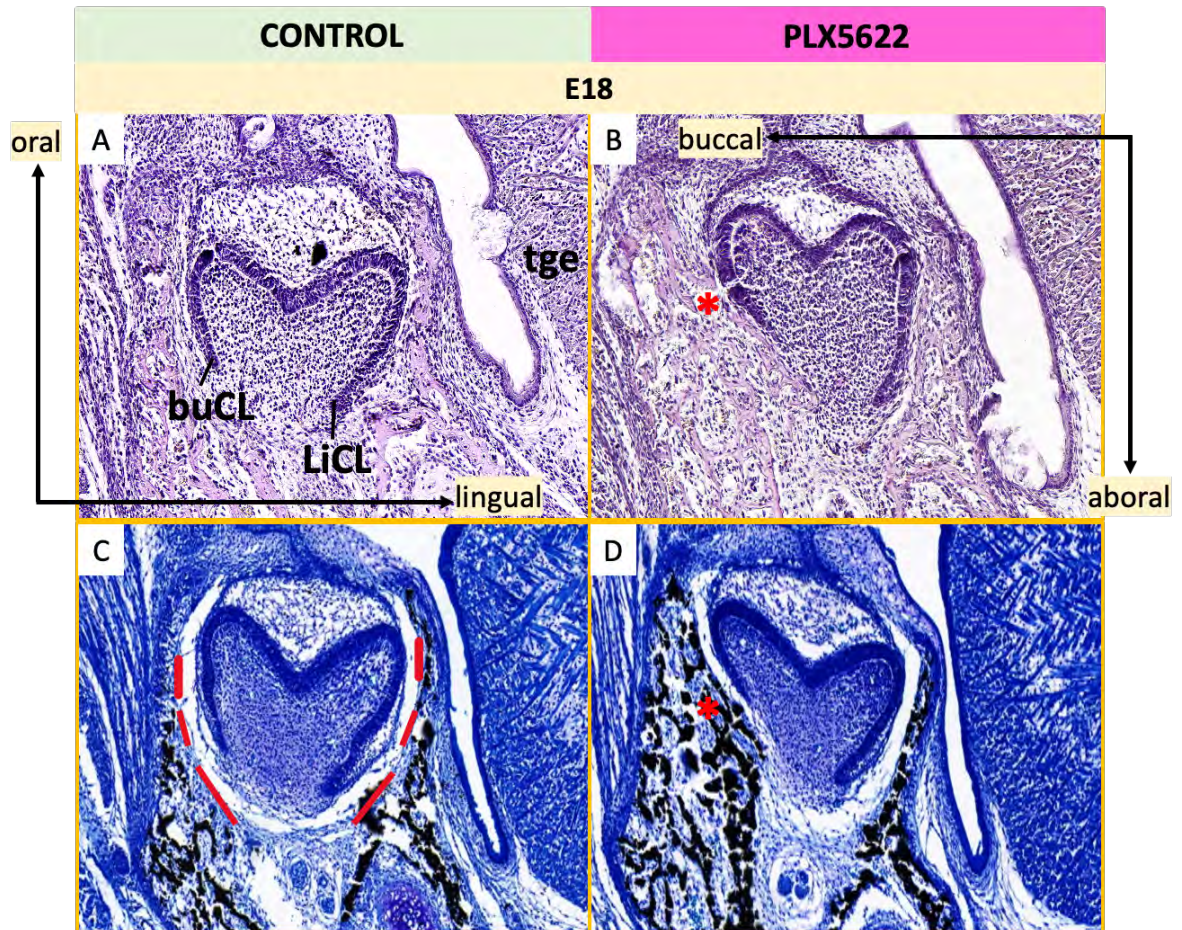


**Figure 3.13. Histological analysis of mandibular first molar at E18.** Coronal sections. Left: Tooth germs in control mice stained with (A) H&E and (C) Von Kossa/tetrachrome. Right: Tooth germs in mice exposed to CSF1R inhibition with PLX5622 *in utero* stained with (B) H&E and (D) Von Kossa/tetrachrome. (B) Constriction in buccal-lingual axis, in comparison to A. (C) Molar germ develops within bony crypt (black). (D) Alveolar bone is in very close contact with the buccal side of the molar germ (\*). *n* = 2 control and PLX5622-treated mice. Buccal cervical loop (buCL), Lingual cervical loop (LiCL), tongue (tge).

incisal ← → apical  
 (distal or anterior) (proximal or posterior)

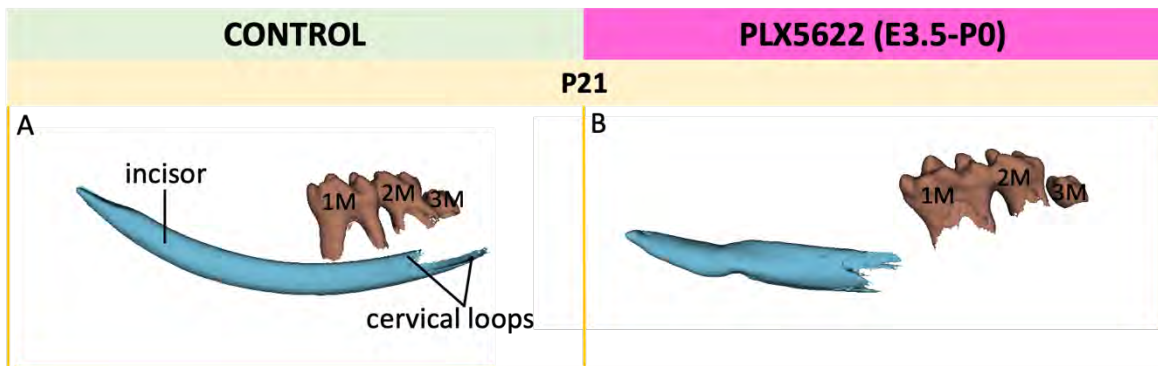


**Figure 3.14. Micro-CT construction of mandibular incisors at P21.** (A) In control mice, the apical end of the incisor elongates posteriorly in the mandible. The labial cervical loop sits at the level just posterior to the third molar. (B) Failure of apical end of incisor to elongate posteriorly in CSF1R-inhibited mice. *n* = 7 to 8 control and PLX5622-treated mice. First molar (1M), second molar (2M), third molar (3M).

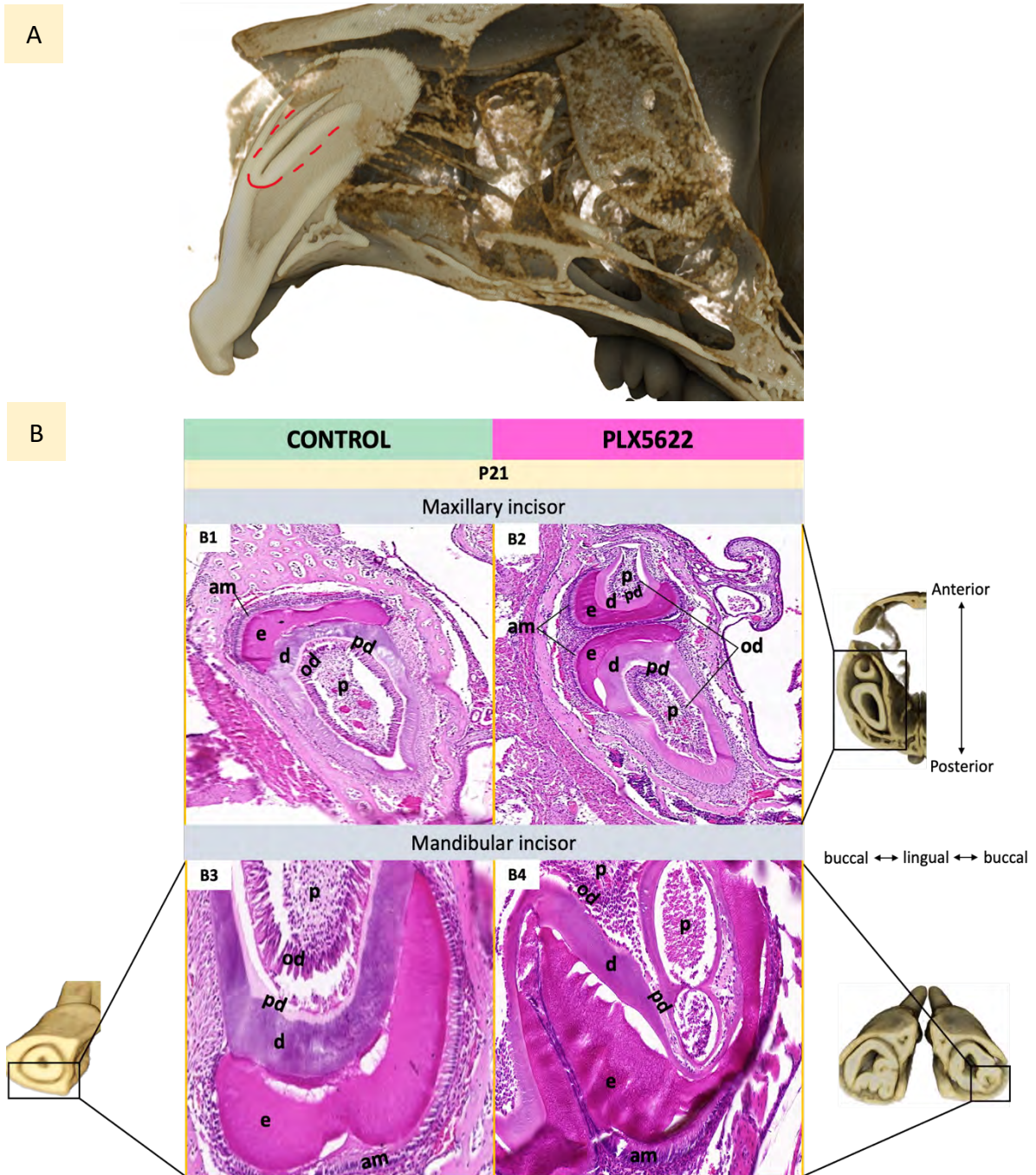


**Figure 3.15. Analysis of erupted teeth at P21.** (A) Micro-CT imaging of CSF1R-inhibited mouse. The maxillary incisor is branched (red lines) on its facial surface, apically. (B) Left: Maxillary (B1) and mandibular (B3) incisors in control mice stained with H&E. Right: Maxillary (B2) and mandibular (B4) incisors in CSF1R-inhibited mice stained with H&E. (B2) Double tooth-like phenotype, in comparison to B1. An ectopic, branched structure with dental cells, enamel, dentin, and pulp is flipped and attached to original incisor. (B4) Invagination of the dentin-enamel junction with grossly disorganized dentin and pulp. *n* = 1 control and PLX5622-treated mouse. Ameloblasts (am), dentin (d), enamel (e), odontoblasts (od), predentin (pd), pulp (p).

Age	H&E		Von Kossa / Tetrachrome		Pollak's Trichrome		Micro-CT	
	n	PLX5622 Phenotype	n	PLX5622 Phenotype	n	PLX5622 Phenotype	n	PLX5622 Phenotype
<b>E18</b>	5	ALL	3	ALL	3	ALL	N/A	
<b>Maxillary Incisor</b>		labial odontogenic infoldings		narrow TBI		data not shown		
<b>Mandibular incisor</b>								
<b>Molar</b>		buccal-lingual constriction; mesial-distal enamel organ narrowing		narrow TBI (on buccal surface)		narrow TBI (on mesial and apical surfaces)		
<b>P3</b>	3	ALL	N/A		3	ALL	N/A	
<b>Maxillary Incisor</b>		apical fragmentation; incisal bend				narrow TBI		
<b>Mandibular incisor</b>		apical fragmentation; no elongation						
<b>Molar</b>		N/A				N/A		
<b>P5</b>	3	ALL	N/A		3	ALL	N/A	
<b>Maxillary Incisor</b>		apical fragmentation; incisal bend				narrow TBI; some recovery (on apical end)		
<b>Mandibular incisor</b>		apical fragmentation; no elongation						
<b>Molar</b>		mesial-distal enamel organ narrowing				N/A		
<b>P21</b>	1 (M)	ALL	N/A		N/A		8*	ALL
<b>Maxillary Incisor</b>		gemination					(4M,4F)	ectopic enamel ridges
<b>Mandibular incisor</b>		dentin-enamel infoldings; disorganized pulp						no elongation; undetectable cervical loops
<b>Molar</b>		N/A						N/A

**Table 1.1. Summary of PLX5622-treated mice.** The numbers (n) of control and PLX5622-treated mice tested at E18, P3, P5, and P21 using histological techniques or micro-CT are shown. Dental phenotypes displayed in the incisors and molars of all PLX5622-treated mice are listed. *Female (F), male (M)*. \*\* n = 7 control and 8 PLX5622-treated mice.

### 3.3 Osteoclast function during early and postnatal stages of odontogenesis

Tooth eruption failure due to defective osteoclastic bone resorption has been suggested to cause the dental abnormalities seen in *Csf1<sup>op/op</sup>* rodents [21, 132]. To determine if osteoclasts are necessary during embryonic odontogenesis in addition to the tooth eruption process postnatally, the TRAP assay was performed. TRAP is strongly expressed by osteoclasts during bone resorption [147]. Therefore, TRAP as a bone resorption marker was assayed to follow osteoclasts in developing incisors and first molars and their surrounding maxillary and mandibular tissues at E18 following morphogenesis and beginning of cytodifferentiation. Osteoclasts were also assayed at P3 and P5 and in CSF1R-inhibited mice exposed to PLX5622 *in utero* between E3.5 and birth.

At E18, TRAP<sup>+</sup> cells were abundant and located in the soft tissue spaces between control tooth germs and the surrounding ectomesenchyme-derived bone (Figure 3.16A; Figure 3.17A; Figure 3.18A). There was generally a higher localization of TRAP<sup>+</sup> cells around mandibular incisor germs than in maxillary incisor germs. TRAP<sup>+</sup> cells surrounded the proximal and distal ends of mandibular incisor germs as well as their labial and lingual surfaces, but higher localization was apparent proximal to the cervical loops (Figure 3.16A). TRAP<sup>+</sup> localization occurred only near the labial surfaces of maxillary incisor germs (Figure 3.17A). In molar germs, the localization was in the soft tissue at the mesial and apical surfaces, in other words distal and aboral to the molar germs (Figure 3.18A).

At P3, the intensity of TRAP staining became more prominent in the soft tissues around incisors and molars. TRAP<sup>+</sup> cells were now heavily evident near the occlusal surfaces, distal

to the incisors and oral to the mandibular molars where the crowns will later exit the oral cavity during eruption (Figure 3.16C; Figure 3.17C; Figure 3.18C). The TRAP<sup>+</sup> cells lining the surfaces of the surrounding bone from within the soft tissues at E18 could be further seen entering the trabecular bone at P3 (Figure 3.16C; Figure 3.17C; Figure 3.18C).

At P5, TRAP<sup>+</sup> cells were still surrounding incisors and molars and lining the bony surfaces, but the general intensity of the staining was less than at P3 and more around mandibular incisors than maxillary incisors (Figure 3.16E; Figure 3.17E). Surprisingly, no TRAP staining was visible on the occlusal (oral) surfaces of molar germs (Figure 3.18E), considering that others have described a greater number of TRAP<sup>+</sup> osteoclasts and their mononuclear precursors at P5 than at P3 in these regions [148].

Strikingly in CSF1R-inhibited mice, no TRAP<sup>+</sup> cells were detected around incisor and molar germs at E18 (Figure 3.16B; Figure 3.17B; Figure 3.18B). Postnatally by day 5, however, TRAP<sup>+</sup> cells slowly repopulated the areas previously observed under control conditions around incisors and molars. At P3, only few TRAP<sup>+</sup> cells surrounded the apical ends of the tooth germs (Figure 3.16D; Figure 3.17D; Figure 3.18D), but the numbers markedly increased at P5 (Figure 3.16F; Figure 3.17F; Figure 3.18F).

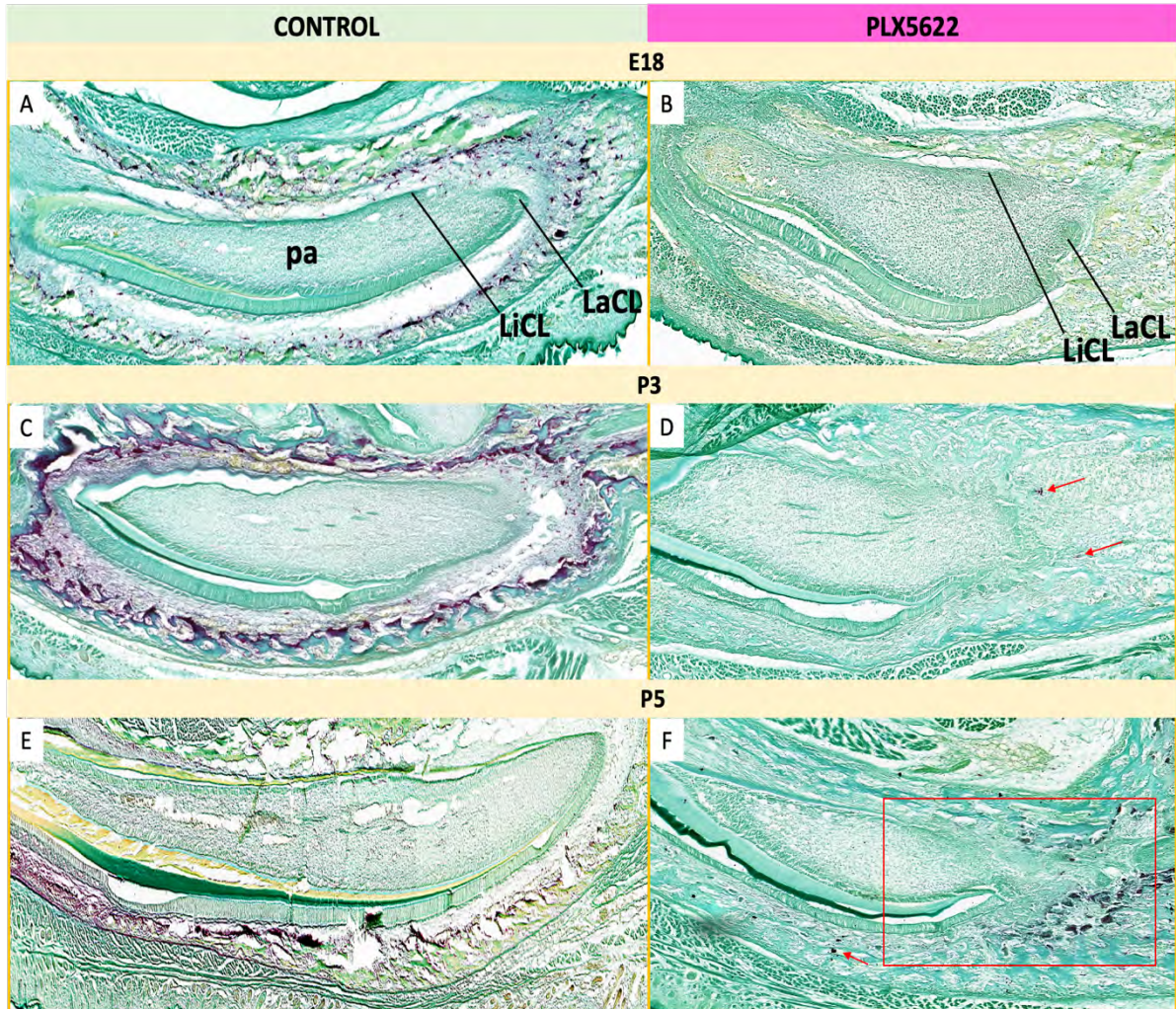
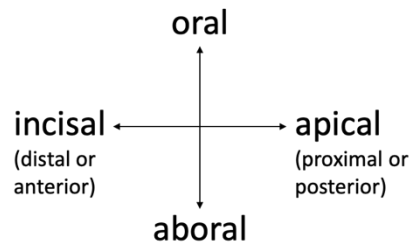


**Figure 3.16. TRAP staining in mandibular incisors at E18, P3, and P5.** (A, C, E) TRAP<sup>+</sup> cells (red/brown) line soft tissue space between incisor germs and surrounding bone in control mice. (B) At E18, no TRAP<sup>+</sup> cells around the incisor germ in the CSF1R-inhibited mouse. (D) At P3, a few TRAP<sup>+</sup> cells (arrows) on the apical side of the incisor germ detected in the CSF1R-inhibited mouse. (F) At P5, a much higher number of TRAP<sup>+</sup> cells (box; arrow) repopulate the tissues surrounding the incisor germ in the CSF1R-inhibited mouse. *n* = 3 to 4 control and PLX5622-treated mice at each age. Dental papilla (*pa*), labial cervical loop (*LaCL*), lingual cervical loop (*LiCL*).

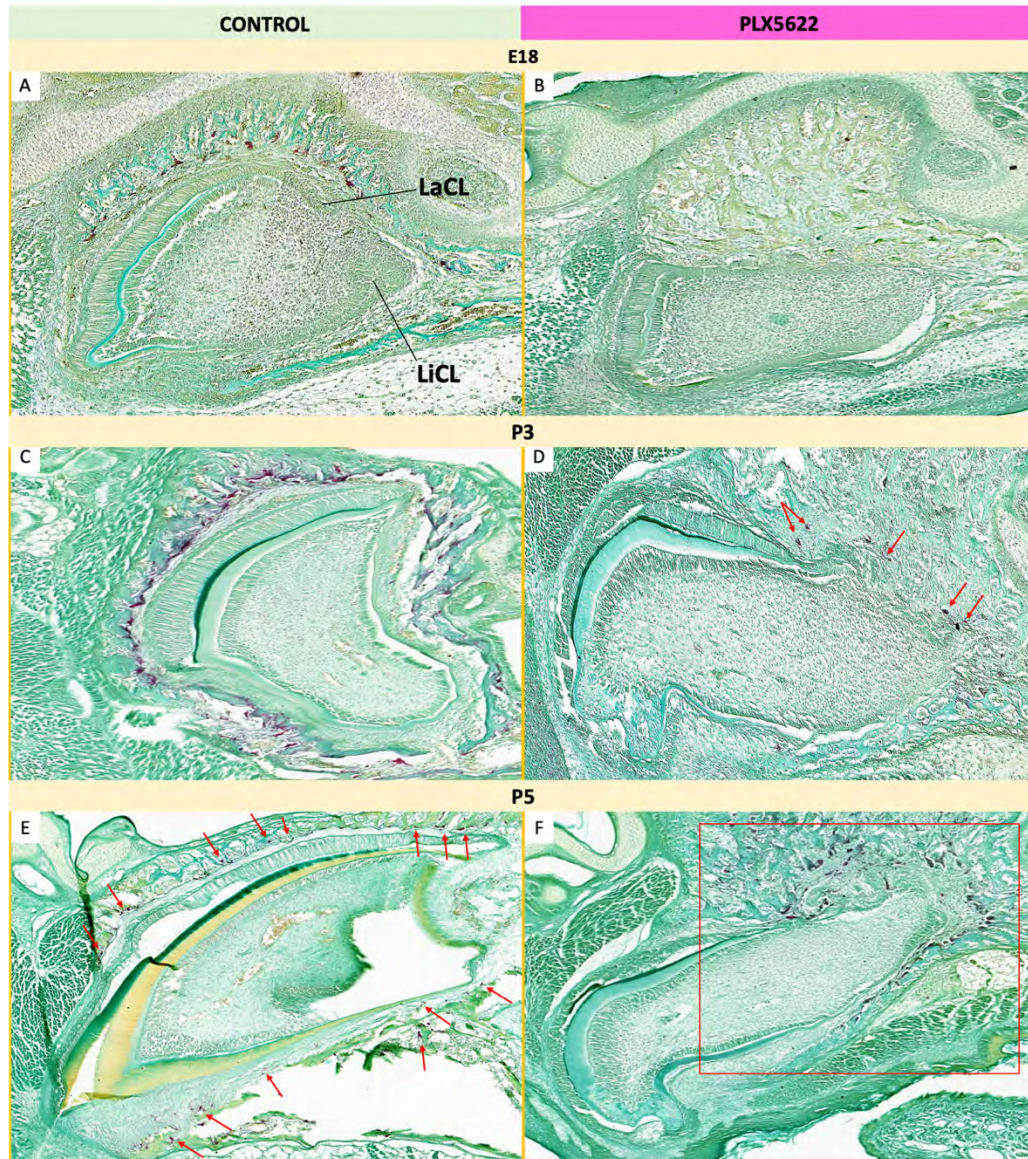
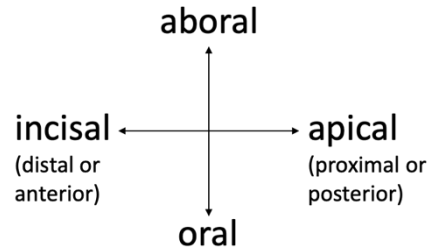


**Figure 3.17. TRAP staining in maxillary incisors at E18, P3, and P5.** (A, C, E) TRAP<sup>+</sup> cells (red/brown) line soft tissue space between incisor germs and surrounding bone in control mice. (B) At E18, no TRAP<sup>+</sup> cells around the incisor germ in the CSF1R-inhibited mouse. (D) At P3, a few TRAP<sup>+</sup> cells (arrows) on the apical side of the incisor germ detected in the CSF1R-inhibited mouse. (F) At P5, a much higher number of TRAP<sup>+</sup> cells (box) repopulate the tissues surrounding the incisor germ in the CSF1R-inhibited mouse. *n* = 3 to 4 control and PLX5622-treated mice at each age. Labial cervical loop (LaCL), lingual cervical loop (LiCL).

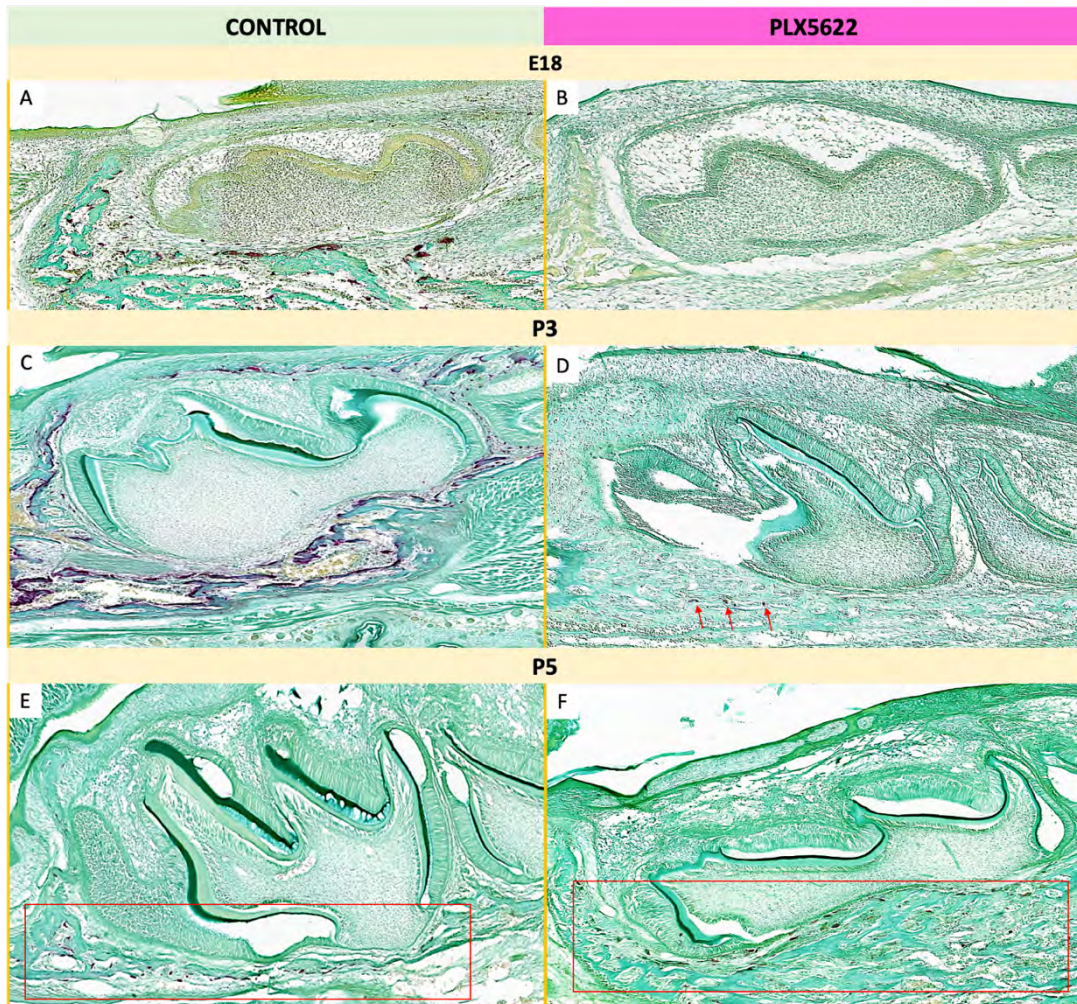
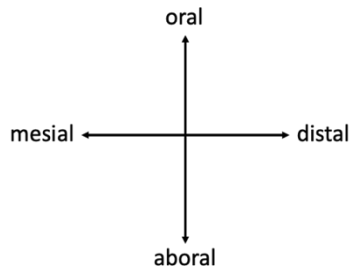


**Figure 3.18. TRAP staining in mandibular first molars at E18, P3, and P5.** (A, C, E) TRAP<sup>+</sup> cells (red/brown) line soft tissue space between molar germs and surrounding bone in control mice. (B) At E18, no TRAP<sup>+</sup> cells around the molar germ in the CSF1R-inhibited mouse. (D) At P3, a few TRAP<sup>+</sup> cells (arrows) aboral to the molar germ detected in the CSF1R-inhibited mouse. (F) At P5, a much higher number of TRAP<sup>+</sup> cells (box) repopulate the tissues surrounding the molar germ in the CSF1R-inhibited mouse. *n* = 3 to 4 control and PLX5622-treated mice at each age.

### 3.4 Postnatal CSF1R inhibition after the completion of odontogenesis

Since mouse incisors erupt continuously due to stem cells located in the cervical loop region, we assessed juvenile mice and studied the effects of CSF1R inhibition on incisor growth. PLX5622 or control diets were administered to CD1 mice at P28 for four weeks. Teeth were then analyzed with micro-CT. Incisors in CSF1R-inhibited occluded normally and no morphological defects were visible (Figure 3.19B) when compared to controls (Figure 3.19A). Enamel, the hardest tissue of the body, appears white on x-rays. In the jaws, enamel formation on the labial surfaces of incisors was unperturbed and resembled the controls (Figure 3.19A', B').

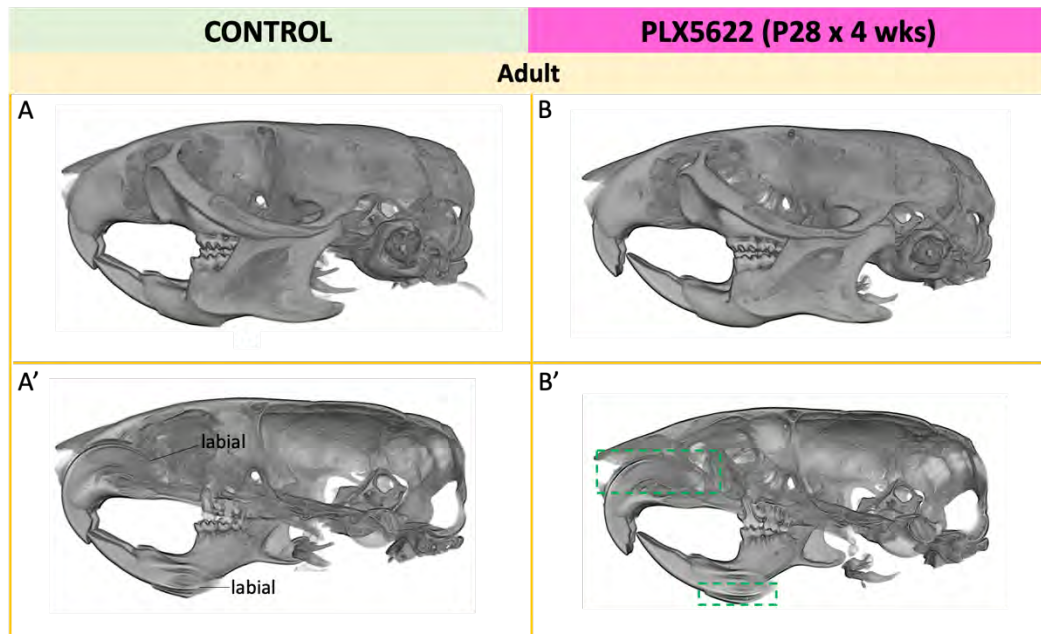


**Figure 3.19. Micro-CT images of adults treated with (A, A') control or (B, B') PLX5622 diet at P28 for four weeks.** Ability for continuous elongation during adulthood is not compromised in CSF1R-inhibited mice. (B) Maxillary and mandibular teeth properly occlude. (B') Newly added enamel on labial surfaces of maxillary and mandibular incisors within the jaws appear normal (green boxes). *n* = 3 control and PLX5622-treated mice.

## Chapter 4: Discussion

### 4.1 Determining when and where CSF1R signaling occurs in odontogenesis

The dramatic morphological changes observed here in the erupted teeth of PLX5622-treated mice must be based on CSF1R signaling within the developing tooth. However, we have now shown that CSF1R is not expressed in the enamel organ during morphogenesis and cytodifferentiation between E13.5 and P5. As such, CSF1R does not directly regulate the shape and growth of the developing teeth. Considering that macrophages residing in the dental pulp during adulthood are initially established in the dental papilla early in development, the positive immunostaining we saw in these tissues must have come from CSF1R<sup>+</sup> macrophages [149]. It is surprising that ameloblasts and odontoblasts did not express CSF1R postnatally, since transcripts in these dental cells have been detected elsewhere [22]. Our results indicate that while transcription of the *Csf1r* gene may occur in ameloblasts and odontoblasts, CSF1R is not translated.

We illustrate that CSF1R<sup>+</sup> cells have a close relationship with the developing tooth. *In vivo*, CSF1R expression increased in the ectomesenchymal tissues directly surrounding the tooth germs as they progressed through morphogenesis (see Figures 3.1 to 3.3). This expression may arise in the DF, since the DFs of rat molars are reported to express CSF1R postnatally [89]. We will need to confirm this using one of the cell surface markers for the DF [86]. CSF1 is also expressed in the DFs of rodent molars [90]. The DF is an ectomesenchymal tissue derived from cranial neural crest cells and has mesoderm-mesenchyme characteristics [78,150]. While it is plausible that CSF1 is expressed by DF cells since it is expressed by mesenchymal-derived osteoblasts, a distinct population of cells residing within or on margins of the DF likely express

CSF1R. There is no evidence of CSF1R expression outside the monocyte/macrophage lineage [151]. Although we found CSF1 and CSF1R to colocalize presumably in the DF region of tooth germs, the receptor may be mediating the paracrine effects of its ligand secreted by DF cells (see Figure 3.2).

#### **4.2 PLX5622 robustness as a CSF1R inhibitor**

Elucidating the role of CSF1R during early odontogenesis was key in this thesis. To approach this, we utilized the CSF1R inhibitor, PLX5622 (Plexxikon Inc.), to permit the inhibition of CSF1R at critical stages of odontogenesis during embryogenesis. PLX5622 is a drug with much higher specificity for CSF1R than other inhibitors of the same class (PLX3397). Additionally, its lower molecular weight and higher lipophilicity makes it easier to cross the placental barrier [152]. Administration of the drug is simple, as it is formulated in animal chow diet and then fed to mice. Pharmacological studies indicate low clearance rates of PLX5622 in a dose-dependent manner such that mice fed once daily at the highest drug dose (PLX5622-1200 ppm chow) have systemic exposure values exceeding 200,000 ng\*hr/mL across 24 hours [160].

The PLX drugs cross the blood-brain barrier and are commonly used in research for microglial elimination in the brain [152]. We have recently shown that 99% of total brain IBA1-stained microglia are eliminated approximately twelve days after the administration of PLX5622 prenatally, and upon drug withdrawal at birth, microglial repopulation to normal levels occurs within seven days [23]. Microglia maintain CSF1R expression throughout development and adulthood, so they make suitable cell markers for the detection of this receptor [134]. It is

reasonable to then think that like microglia, other cells dependent on CSF1R for development are eliminated by PLX5622 and will repopulate respective tissues with similar timelines upon drug withdrawal. Indeed, PLX5622 is not microglia specific and is shown during adulthood to affect other cells of the monocyte/macrophage lineage [153]. We have also demonstrated the robustness of PLX5622, since its administration between E3.5 and E18 led to the loss of CSF1R staining in odontogenic regions in comparison to controls (see Figure 3.5). This loss may be direct results of an earlier decrease in the number of proliferating CSF1R<sup>+</sup> cells and subsequent apoptosis of cells requiring CSF1R activity for survival. Measuring the proliferation of CSF1R-stained microglia at E10.5, when these cells are first detectable in the developing brain, and apoptosis of CSF1R-stained cells around developing teeth at later embryonic time points may explain the mechanism of cell ablation induced by PLX5622. The mechanism of PLX5622 is reversible, as demonstrated through IF experiments at P3 and P5 in which CSF1R<sup>+</sup> cells gradually repopulated the craniofacial regions after withdrawal of PLX5622 at birth (Appendix G).

While genetic models to assess phenotypes are important, they pose some challenges to study the questions proposed here. *Csf1r*<sup>-/-</sup> mice die early in the postpartum period, thereby precluding a comprehensive analysis of dental phenotypes induced at early odontogenesis [154]. Because *Csf1r*<sup>-/-</sup> mice are osteopetrotic and do not erupt their teeth, we cannot distinguish between the effects associated with tooth eruption failure and direct effects on odontogenic tissues. The tooth eruption process is unperturbed in mice treated with PLX5622 *in utero* until birth [23]. Hence, all PLX5622-treated animals here had erupted teeth, allowing us to elucidate the role of CSF1R in odontogenesis independent of its role in osteoclast-

mediated tooth eruption. PLX5622 as a convenient pharmacological system for our CSF1R inhibition studies circumvented the drawbacks of genetic models.

### **4.3 An overview of the effects of embryonic and postnatal CSF1R inhibition on teeth in juvenile and adult mice, respectively**

In a previous study done by our group, morphological defects in the erupted teeth of juvenile mice exposed to PLX5622 *in utero* between E3.5 and birth were briefly described [23]. Compared to controls, incisor crowns were smaller and notched, lacked curved morphologies, and contained ectopic enamel ridges on labial surfaces. Here, we have used micro-CT imaging and histological methods at P21 to further observe these previously described dental abnormalities in CSF1R-inhibited mice.

In rodents, incisor morphogenesis occurs longitudinally along the labial-lingual axis mainly by the proximal (posterior) extension of proliferating cells in the IEE and dental papilla at apical ends [59]. Inhibition of CSF1R with PLX5622 during morphogenesis negatively affected incisor size due to an obvious lack of extension at the apical ends (see Figure 3.14). The previously described notching and ectopic enamel ridges in the incisor crowns of CSF1R-inhibited mice are possibly a single abnormality rather than distinct abnormalities contributing to the loss of normal curved morphology. Notching may be secondary to the formation of the ectopic enamel ridge since the former deformity was located near the incisal edge immediately distal (more anterior) to the latter deformity on the labial surface [23]. Here, we had taken sections from the proximal (posterior) regions in mandibles of CSF1R-inhibited mice at P21 and additionally found unusual infoldings in the enamel-dentin junctions on the labial surfaces

of incisors (see Figure 3.15B4). We suggest that these dental infoldings within the jaw may reflect the ectopic enamel ridges visible on the crown facial surfaces.

Variability of dental abnormalities among the maxillary and mandibular incisors in CSF1R-inhibited mice was rather surprising. Maxillary incisors displayed a double tooth phenotype rather than enamel-dental infoldings (see Figure 3.15B2). Since the formation of double teeth in the maxilla of CSF1R-inhibited mice did not change the overall tooth number, the smaller ectopic tooth must have formed by gemination or from the branching of the original incisor [155]. Indeed, both structures shared the same DF. We revealed that the geminated structure was a small ectopic enamel ridge rather than a fully developed incisor, thus it is possible this dental abnormality originated from the same process that caused the enamel-dentin infoldings in mandibular incisors but with different severity (see Figure 3.15A). Differences between upper and lower jaw bone architecture and their responses to occlusal forces suggest that there may be accordant differences between the development of their respective dentitions [156,157]. Certainly, dissimilarities in apical growth and incisal end shapes between mandibular and maxillary incisors have been noted in rodents [158]. This may explain why incisors in PLX5622-treated mice manifested unique dental abnormalities observed at the tissue level. Deficiencies in CSF1R signaling due to PLX5622 clearly caused tooth shapes and sizes to deviate but based on our observations alone at P21, the mechanisms involved are unclear. We expected CSF1R expression in the dental epithelium, so we were surprised to not find it. Another CSF1R-dependent mechanism likely regulates dental epithelial morphogenesis indirectly.

In addition, we were interested in knowing if CSF1R has any role in continuous incisor growth in mice. Labial cervical loops house the dental epithelial stem cells for ameloblast differentiation and thus enable the continuous growth of incisors during adulthood [29]. At P21, the labial and lingual cervical loops in the incisors of CSF1R-inhibited mice were not well demarcated (see Figure 3.14). Our interpretation is that, like FGF10, CSF1R expressed in the dental papilla may regulate cervical loop formation during early morphogenesis [59]. However, its immunostaining in the dental papilla was rather faint and scattered and likely represented macrophages (see 4.1). Embryonic disruptions in the labial cervical loops in CSF1R-inhibited mice may prevent enamel renewal, but this would need to be tested. We showed that in mice treated with PLX5622 at P28 for four weeks, enamel production and the occlusion of incisors were normal (see Figure 3.19). Since continuous incisor growth was unaffected by CSF1R inhibition, CSF1R has no role in the maintenance of dental epithelial stem cells.

#### **4.4 An overview of the effects of embryonic CSF1R inhibition on odontogenesis in E18 and neonatal mice**

As far as we are aware, no study to date has described the histopathology of tooth germs in *Csf1<sup>op/op</sup>* and *Csf1r<sup>-/-</sup>* mice prenatally. We wanted to better understand the effects of CSF1R in tooth morphogenesis, so we analyzed tooth germs immediately after they had undergone morphogenesis using histology. Teeth began developing abnormalities *in utero* during early odontogenesis at the time of CSF1R inhibition. Cervical loops of incisors had formed at E18 in the absence of CSF1R signaling, but they could no longer be detected postnatally when CSF1R<sup>+</sup> cells were repopulating after PLX5622 withdrawal. Therefore, we reject the

possibility that CSF1R has a role in cervical loop formation (see Figure 3.6; Figure 3.7; Figures 3.9 to 3.11). Alternatively, the eventual disturbance of properly formed cervical loops was likely a secondary effect of CSF1R inhibition during embryogenesis rather than a direct effect in odontogenic tissues. At the early postpartum period, apical ends of incisors in CSF1R-inhibited mice were fragmented and had failed to grow posteriorly in the jaws. These fragmentations resembled the multiple tooth-like structures branching off the apical ends of unerupted incisors in *Csf1<sup>op/op</sup>* mice [21]. Dental epithelium and dental ectomesenchyme near the apical ends have proliferative capacities, enabling the posterior growth of incisors [133]. This suggests that the more anterior (distal) portions of incisors alone cannot support posterior growth, and thus may explain why incisors that had been detached from their apical ends were atrophic in CSF1R-inhibited mice.

Although molar germs were less malformed relative to incisor germs in CSF1R-inhibited mice, narrowing of their buccolingual widths at E18 was rather interesting (see Figure 3.13). This matches the morphological defect in molars observed at P21 in our previous study [23]. Roots of the molars at P21 are also reported to show taurodontism, which needs to be explored further [23].

Cytodifferentiation of specialized dental cells occurs prenatally while the production of enamel and dentin continues postnatally. Ameloblasts and odontoblasts observed postnatally in the unerupted teeth of *Csf1<sup>op/op</sup>* mice are atrophic, flat (lack normal columnar shapes), and express less amelogenin and dentin matrix protein 1 (DMP1), respectively, than normal teeth [22]. In contrast, we show that ameloblasts and odontoblasts were normal prenatally and postnatally in the tooth germs of mice exposed to CSF1R inhibition *in utero* until birth. This suggests that

CSF1R does not have a role in early ameloblast and odontoblast differentiation, and that the cellular defects in *Csf1<sup>op/op</sup>* mice must have arisen from osteoclast deficiencies in the surrounding ectomesenchyme of developing teeth. However, it is possible CSF1R is important for dentin and/or enamel matrix protein production, since the dentin-enamel junctions in CSF1R-inhibited mice appeared faulty (see Figure 3.9D, H).

#### **4.5 The relationship of CSF1R, teeth, and alveolar bone during development**

Understanding the relationship between the developing tooth and alveolar bone is important for explaining why CSF1R localized in tissues encompassing the tooth germ proper during odontogenesis. The development of alveolar bone occurs concurrently with the development of teeth in jaws [38]. Using bone-based histology methods, we found that upon CSF1R inhibition, the surrounding alveolar bone trabeculae had encroached into the tooth germ space, especially at the apical ends during morphogenesis (see Figure 3.6; Figure 3.7; Figure 3.12). After removal of PLX5622, tooth germs at P3 and P5 were severely interrupted and encased by bone (see Figures 3.9 to 3.11). Our interpretation is that the effects of CSF1R inhibition on tooth germs were prolonged immediately after birth due to insufficient CSF1R signaling, since CSF1R<sup>+</sup> cells do not fully repopulate until seven days after PLX5622 removal [23].

Our study of odontogenesis highlights the importance of osteoclasts not only at postnatal times when teeth are being primed for eruption but also during embryogenesis. Like the pattern of CSF1R expression, osteoclasts were localized around tooth germs undergoing morphogenesis and were absent in CSF1R-inhibited mice (see Figures 3.16 to 3.18). Indeed, action of bone-resorbing osteoclasts during embryogenesis creates spaces in the developing alveolar bone so

that tooth germs can develop within crypts [159]. Medial to incisor germs is a calcified cartilaginous structure called Meckel's cartilage that serves as a template for mandible development [160]. It is temporary and resorbed by osteoclasts, starting at the lateral side around E18 [160-162]. We noted areas of unresorbed Meckel's cartilage due to CSF1R inhibition (see Figure 3.8). This indicates an overall lack of osteoclast-mediated bone resorption in the craniofacial regions of CSF1R-inhibited mice during odontogenesis.

CSF1R is constitutively expressed in osteoclasts and is critical for osteoclast differentiation, survival, and function (see Figure 1.5). We propose that the CSF1R<sup>+</sup> cells in the soft tissue regions between the developing tooth and alveolar bone are osteoclasts. Treatment with CSF1R inhibitor PLX5622 between E3.5 and birth prevented the formation of functional osteoclasts altogether, thus a lack of osteoclast-mediated bone resorption around tooth germs is likely a mechanism for the disruption of tooth morphogenesis. PTHRP is expressed in the enamel organ and is required for the formation of an eruption pathway [195,163]. PTHRP knockout and knockdown studies show that at embryonic time points osteoclasts forming around tooth germs are impaired, leading to the destruction of tooth germs by the invasion of alveolar bone [164,165]. No abnormalities in the dental cells were noted in these mice, which matches our findings in CSF1R-inhibited mice.

#### **4.6 Conclusion**

For the teeth to erupt, osteoclasts must resorb the coronal aspects of alveolar bone encasing tooth germs. In *Csf1<sup>op/op</sup>* and *Csf1r<sup>-/-</sup>* mice that have osteoclast deficiencies, the eruptive pathway is not formed postnatally. In the former model, dental abnormalities in the unerupted

teeth are also observed. To determine whether these dental abnormalities are direct effects of CSF1R in early odontogenesis or secondary effects from failure of tooth eruption, we clarified the relationship between developing teeth and alveolar bone using a pharmacological model of CSF1R inhibition during morphogenesis.

Our results support the hypothesis that CSF1R has a role in tooth morphogenesis; though, it is likely indirect. The time-specific inhibition of CSF1R during embryogenesis did not seem to diminish the developmental potential of tooth germs. Rather, disturbed morphology, especially of the incisors, was caused by an abnormality in bone resorption initiated early in development. Our notion that the CSF1R<sup>+</sup> cells stationed around tooth germs were osteoclasts is reinforced by a previous study, which found TRAP<sup>+</sup> osteoclasts in regions between molar germs and alveolar bone [166]. Notably, this soft tissue region containing the DF is identified as the tooth-bone interface (TBI) [146,166]. As such, we suggest that the role of CSF1R in early odontogenesis is confined to the TBI, where it likely regulates the osteoclast-mediated resorption of bony crypts forming around the growing tooth germs. When this mechanism fails, the tooth germ expands into the alveolar bone and loses normal morphology because it no longer has adequate space to grow. Disturbed tooth morphology cannot be spontaneously rescued immediately after removal of PLX5622 at birth, thus indicating the requirement of CSF1R during a critical odontogenic window.

#### **4.7 Future directions**

We have underscored the role of CSF1R in the indirect regulation of tooth morphogenesis. It is necessary to confirm that CSF1R lacks a direct role in early odontogenesis. Further study

will require tooth germs be separated from their bony tissues and grown independently in explant cultures with PLX5622. The developmental potential of the IEE and cervical loops from CSF1R-inhibited tooth germs will be tested in proliferation assays using an anti-Ki67 antibody. The nuclear protein Ki67 is a well-established proliferation marker, as it is active throughout the cell cycle except in the G0 phase [167]. Tamoxifen-inducible *Cre*-driver mice using the *Keratin 14 (K14)* promoter may also be used to delete *Csf1r* in the growing dental epithelium for investigating its direct *in vivo* effects during tooth morphogenesis.

Ameloblasts and odontoblasts in our CSF1R-inhibited mice display no morphological abnormalities, except at regions of direct contact between tooth germs and surrounding bone. Using laser capture microdissection and RNA-Seq technology, differential gene expression can be measured in isolated ameloblasts and odontoblasts to determine the regulation of CSF1R in cytodifferentiation and enamel and dentin matrix production. Whether CSF1R is expressed in dental cells will need to be confirmed with immunoblotting.